3-Dimensional NXN Passive Optical Star Coupler Based on the Exact Eigenmode Coupling and Diffraction Theory

By

Ken Koon-Hung Lee, B.A.Sc.

A dissertation submitted to the
School of Graduate Studies and Research,
University of Ottawa,
in partial fulfilment of the requirements
for the degree of
Master of Applied Science (Electrical Engineering)

Ottawa-Carleton Institute for Electrical Engineering
Department of Electrical Engineering
Faculty of Engineering
University of Ottawa

ISBN 0-315-80001-1

UNIVERSITÉ D'OTTAWA
UNIVERSITY OF OTTAWA

Abstract

A technique for a 3-Dimensional passive NxN optical star coupler is described. 3-Dimensional antiresonant reflecting optical waveguides (ARROW) are analyzed and utilised as the input and output waveguides of the NxN coupler. The effective Index Method will be employed to replace the 3-Dimensional ARROW waveguide by an equivalent slab waveguide with its refractive index profile determined by the geometrical shape of the ARROW Waveguide. In the slab waveguide analysis, the input waveguides are coupled to their neighbours. The interaction of the waveguides is described in terms of the normal modes. The resultant field distribution is then diffracted into the free space region which separates the input and output sections. The radiation illuminates the receiving aperture from which the receiving waveguide branches into N different individual output elements, each output element obtaining equal power levels. Different types of loss such as bending loss, spill-over loss, mismatch loss, reflection loss were analyzed and estimated for N=5. A 5x5 star coupler with a transmission efficiency of 56 % at a wavelength of 1.3 μm is achievable.

Acknowledgements

I wish to express my sincere gratitude to my academic supervisor Dr. Willem Steenaart for his scientific guidance and moral support during the course of the program.

The help and advice from Dr. M. Tabiani, University of Ottawa is greatly appreciated.

I am thankful to Dr. J.Chrostowski from the Photonics and Sensors Section of the National Research Council of Canada for the useful discussions and advice provided.

Many thanks to all professors, colleagues and friends at the department of Electrical Engineering, University of Ottawa, for the good academic atmosphere and the encouragement during the period of my studies.

This research was partially supported by the Telecommunications Research Institute of Ontario, Photonic Networks and Architectures.

Table of Contents

List of Figures

List of Tables

Chapter 1

Introduction

1.1 Motivation

The single-mode-fibre passive star coupler is a key component in many architectures of high speed optical local-area networks. Ideally, an N x N star coupler divides the power entering any one of its N input ports equally among its output ports. However, there will be excess power loss due to absorption and scattering. The N x N star can serve as the central node in an N-user local area network, where each user would be connected by the fibres — one for transmission to the input side of the star, and the other for reception from the output side of the star. This creates a broadcast-type local-area network, where a message transmitted by any user can be received by all users.

The main advantage of the star over the bus architecture is its small excess loss. The excess loss of an N-star increases only logarithmically with N, while that of an N-user bus increases linearly with N. The difference in loss can be significant for large values of N [1].

A well known technique, which can be used to realize arbitrarily large N, involves the interconnection of a large number of elementary 3-dB couplers [1]. The complexity of such an approach increases logarithmically with N. Dragone [2] considered a different approach. The NxN star coupler is realized in free-space using two arrays, each connected to N single-mode fibres. Power transfer between the input

and output arrays is accomplished through radiation based on Fourier optics. By exciting the input power waveguide successively in a linear phase progression, one of the Bloch modes [2] of the input waveguide can be produced. The results show that if the input waveguide array is in the form of a very gradual transition, it is possible to transform approximately each Bloch mode into a plane wave, thus causing most of the input power to be diffracted in the central zone of the array far-field.

In this thesis, we investigated the field distribution for an N-waveguide coupler in terms of the normal modes [3]. If the individual isolated waveguide contain single modes, the N-waveguide coupler has N normal modes. By solving Maxwell's equations in each waveguide and making use of the fact that the normal modes are either symmetric or anti-symmetric in a symmetric waveguide system, the field distributions of normal modes can be obtained. When the waveguide parameters (transverse and longitudinal propagation constant) vary in the direction of propagation, the normal modes of the structure will be replaced by the concept of a locally normal mode [4].

Moreover, for a waveguide structure slowly varying with propagation distance, negligible power transfer occurs between the normal modes [5]. Thus, power entered into the first-order local mode will end up in the first-order local normal mode.

Strictly speaking, a uniform plane wave does not exist, because a source infinite in extent would be required to create it, and practical wave sources are always finite in extent [6]. If a source is far enough away, the wavefront becomes almost spherical; and a tiny portion of the surface of a big sphere is very nearly a plane. Thus, electromagnetic radiation can approximate the ideal uniform plane wave.

Furthermore, it is observed that the plane wave weighting coefficients are given by the Fourier transform of the beam transverse distribution before diffraction [7].

Last but not least, for a branching waveguide with refractive index and separation

symmetry, the normal modes will maintain a stage of evenly dividing their power between the branches at any separation. Thus, the received power will be distributed to the output ports evenly [8].

Applying the concepts from the above paragraph, four different regions in the couplers can be designed as shown in Fig.4.1 (p.31). The uncoupled region is used to allow input signals from the optical fibres to couple to the device without any influence from its neighbours. In the coupled region, coupling between the adjacent input waveguide will produce a different field distribution as a function of waveguide spacings and coupling length. In the transition region, the input waveguides merge into a single waveguide slowly to allow the input signal to illuminate the transmitting aperture no matter which input waveguide provides the input power. In the diffraction region, the plane wave coefficients are given simply by the Fourier transform of the beam transverse distribution right after the input waveguides merge together. After diffraction, the illuminated receiving waveguide is branched into N waveguides. Each output waveguide is supposed to carry the same power if the index symmetry is valid.

1.2 Contribution

Our contribution is in the following areas:

1. The effective index method was applied to replace the 3-Dimensional ARROW Waveguide by an equivalent slab waveguide whose refractive index profile is determined by the geometrical dimensions of the planar ARROW Waveguide. Thus, we succeeded in converting the 3-Dimensional NxN star coupler into a 2-Dimensional problem.

2. The coupling between the input waveguides was analyzed by the exact eigenmode theory [9]. The solution is expressed as a sum of forward-travelling eigenmodes, each of which is an exact solution of the scalar waveguide equation. We derived the guidance condition, the expression which indicates the relation of propagation constant to the waveguide width and spacing. ([10] did not obtain the correct

expression.)

3. The computer program was developed to calculate the propagation constants, with different waveguide spacings, as the input waveguides merge into the diffraction region.

4. The model was developed to express the input power to any input waveguide in terms of normal modes. These expressions have been derived for n=2 [11].

5. The computer program to perform the Fourier transform was developed such that the field patterns can be calculated after the diffraction.

6. Simulations were performed to vary the transition and diffraction regions to minimise the excess loss.

1.3 Outline of the Thesis

In Chapter 2, an analysis of a planar ARROW waveguide is presented. Structure, operation theory, optimum dimensions for minimum loss, and loss in ARROW waveguide are discussed. Geometrical optics and elementary ray methods are presented to analyze the propagation, including the loss, in ARROW waveguide and the effective refractive index for different dimensions. Moreover, transmission line and transverse resonance methods are used to calculate the loss in the ARROW waveguide and the effective index for different dimensions.

In Chapter 3, the effective index method is employed to replace the 3-dimensional ARROW by an equivalent slab waveguide whose refractive index profile is determined by the geometrical dimensions of the planar ARROW waveguide. The ability to convert a 3-Dimensional problem into a 2-Dimensional one is the main feature and advantage of the method. Thus, we succeeded in converting the 3-Dimensional NxN star coupler into a planar NxN star coupler.

The design of the planar NxN star coupler is presented in chapter 4. The refractive indices are mainly taken from Chapter 3. The NxN star coupler is realized in free-space using two arrays, each connected to n single-mode fibres. Four different

regions in the couplers can be designed as shown in Fig.4.1 (p.31).

Final conclusions and recommendations to the thesis are presented in chapter 5. Other numerical methods, such as the finite element method, can replace the Effective Index Method. The use of a large number of input and output waveguides (N>5) is suggested for future research.

Chapter 2

Analysis of an Anti-Resonant Reflecting Optical Waveguide (ARROW)

2.1 Introduction

In recent years much research work has been directed towards the construction of single-mode, low-loss optical waveguides formed on a planar Si substrate. Many optical devices such as directional couplers, filters, switches have been built on Si substrate. Moreover, this type of structure can integrate both optical and electrical circuits on a single wafer. One common approach is the formation of waveguide on a Si substrate by depositing another dielectric material such as Si_3N_4, or AS_2S_3 glass or $Si_{1-x}Ti_xO_2$. All these dielectrics have a substantially higher refractive index than that of SiO_2. However, the doped SiO_2 or the deposited dielectric layers may be very lossy compared to pure SiO_2. In addition, a considerable thickness of SiO_2 (typically more than 4 μm) is required to minimize radiation losses because of the evanescent field in the Si substrate, with a refractive index from 3.5 to 3.8.

A novel waveguide, an anti-resonant reflecting optical waveguide (ARROW) has been introduced [12]. The configuration of the ARROW waveguide can reduce radiation loss into the Si substrate substantially, without using total internal reflection. In fact, optical confinement is based on anti-resonant reflections, as in a Fabry-Perot interferometer [13]. The Fabry-Perot interferometer consists of an infinite plane-parallel

plate (core) of thickness d and refractive index n_c. Let a plane wave be incident on the medium at an angle to the horizontal, as shown in Fig.2.1. The phase shift due to propagation along the length of path connecting points A and C is given by

$$\psi = 2k_0 n_c d \sin\xi_c \qquad (2.1)$$

where

k_0 is the wavenumber in vacuum (μm^{-1})

ξ_c is the propagation angle in the core (radians)

d is the core thickness (μm)

let us consider the transmission characteristics of a Fabry-Perot interferometer. The interferometer resonates (the transmission is unity) when the phase shift ψ is an integral multiples of 2π. That means the resonances occur over a narrow band of frequencies, the antiresonances are spectrally broad.

These waveguides exhibit low loss in the fundamental TE mode with good loss discrimination against higher order modes.

2.2 ARROW Waveguide Structure

The structure of the ARROW is shown in Fig.2.2. A core is made of SiO_2. The core is bounded on the upper surface by a low-index medium (air) to produce total internal reflection and it is bounded on the lower surface by an interference cladding which is composed of a high index layer (1st cladding), a Si layer and a low index (2nd cladding), SiO_2 layer. Thus, light propagates through the core by repeated total internal reflection at the upper air/SiO_2 boundary and extremely high reflection from the interference cladding when the thicknesses of the interference cladding layers satisfy the anti-resonant condition. Under the anti-resonant condition, maximum reflection occurs in the cladding layers i.e. most of the light energy is reflected back to the core region. If the core layer is thick enough, the fundamental mode has a negligible energy in the air, and the glancing incident angle shown in Fig.2.2 can be approximated by

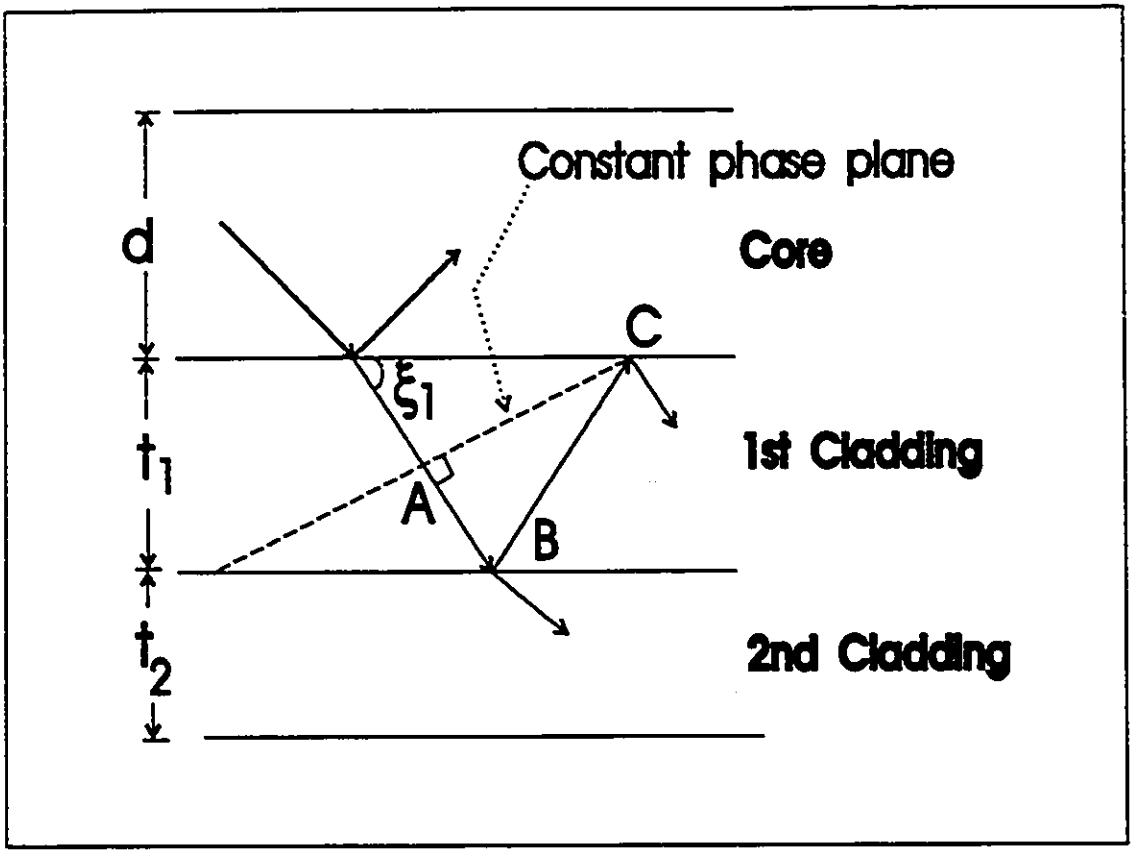

Fig.2.1: Reflection of the Plane Wave Through the Fabry-Perot Interferometer in ARROW Waveguides

$$\sin\xi_c = \frac{\lambda}{2n_c d_e} \tag{2.2}$$

The detailed derivation of equation (2.2) is given in Appendix A.

It has been shown that a plane wave incident upon a less dense medium at an angle greater than the critical angle experiences not only total internal reflection but also a phase delay (shift) that is a function of incident angle. To obtain a zig-zag ray model of light propagation in the waveguide that is consistent with the flow of energy, we have to incorporate the Goos-Hänchen shifts at the core-air and core-cladding interfaces, as first suggested by Burke [14]. A sketch of this ray model with lateral shifts and ray penetration depths is shown in Fig.2.3. As a consequence of the ray penetration, the waveguide

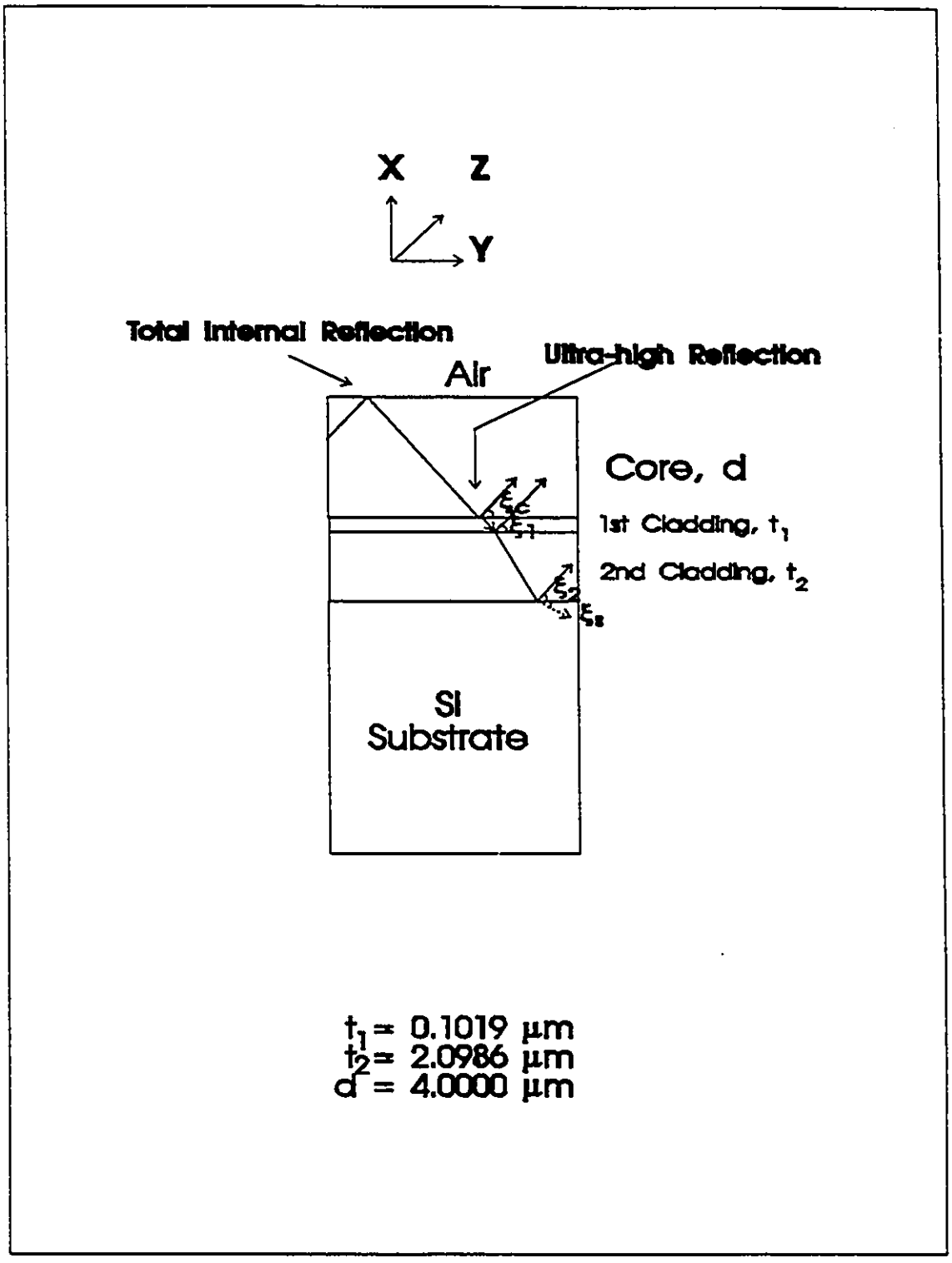

Fig.2.2: Structure of a Planar ARROW Waveguide

appears to possess an equivalent core thickness, d_e.

$$d_e = d + \frac{\lambda}{2\pi(n_c^2 - n_0^2)^{1/2}} \tag{2.3}$$

The derivation of equation (2.3) is given in Appendix B.

The optimum structure (thickness of the cladding layers) to obtain minimum loss for fundamental mode has been formulated [15] and [16]. In a Fabry-Perot interferometer, the phase shift in a cladding between two partial waves can be expressed in terms of thickness. When the phase shift is $\pi/2$, the reflection is unity. Therefore the optimum cladding layer thickness can be formulated to give maximum reflection (see appendix C).

$$t_1 = \frac{\lambda}{4n_1}(2L_1 + 1)\left[1 - \left(\frac{n_c^2}{n_1^2}\right) + \frac{\lambda^2}{4n_c^2 d_e^2}\right]^{-1/2} \tag{2.4}$$

$$t_2 = d_e\left(\frac{1}{2} + L_2\right) \tag{2.5}$$

where

L_1 and L_2 = 0,1,2,3,4.....

n_1 is the refractive index of the first cladding layer

The detailed derivations of the optimum thickness of the first and the second cladding are given in Appendix C & D respectively. The optimum structure which give minimum loss is given in Fig.2.4. There is one important assumption for the derivation of the optimum cladding layers. The core thickness must be large compared to the wavelength of light such that $d > \lambda/2n_c$ where λ is the wavelength of light in vacuum and n_c is the refractive index in the Si core.Thus, the fundamental mode has a negligible evanescent tail in the air. The typical value of the Si core thickness is about 4 μm.

2.2.1 TE Fundamental Mode Profile in ARROW

Let us attempt to find TE-mode waveguide solutions, which by definition have the electric

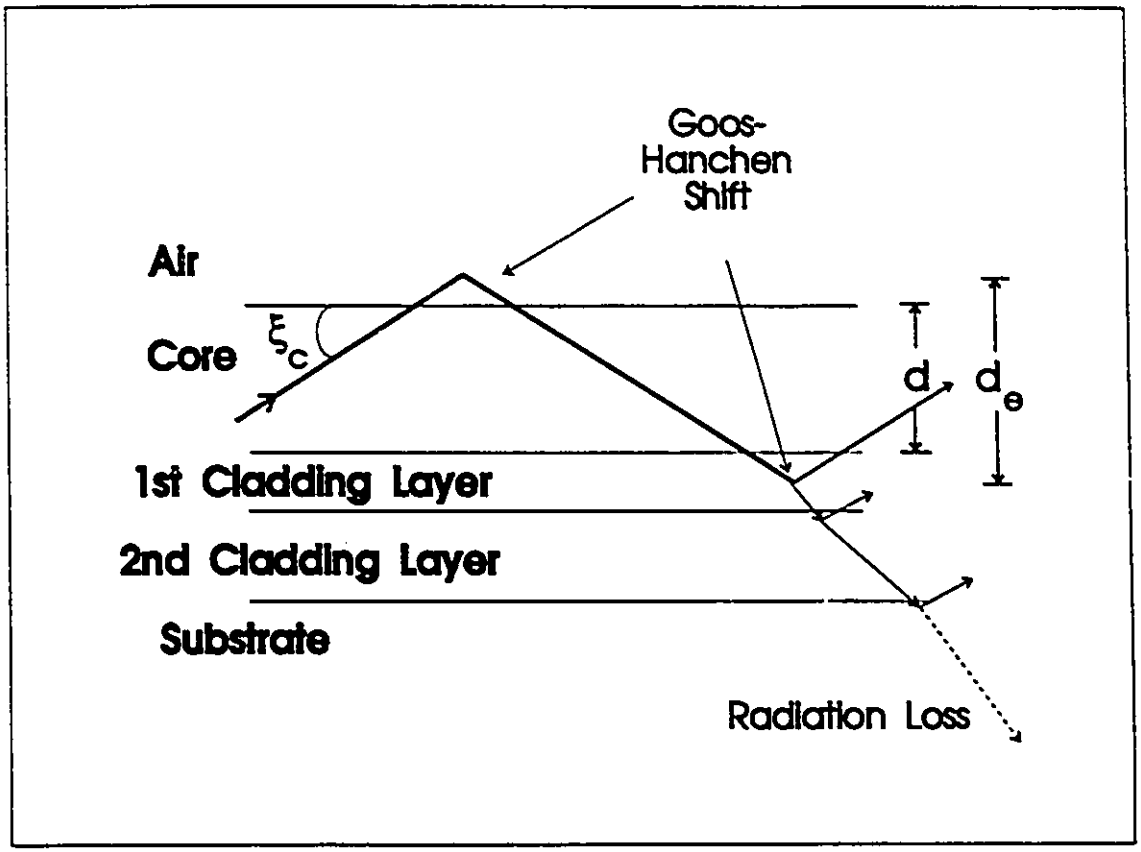

Fig.2.3: Ray-Picture of Zig-Zag Light Propagation in ARROW Waveguide

field polarized along y with propagation in z direction as shown in Fig.2.4. The field component E_y of the TE mode obeys the wave equation as:

$$\nabla^2 E_m(x,y,z) + k_0^2 n_m^2 E_m = 0 \qquad m=1,2,3,.. \tag{2.6}$$

where m refers to the different layers of ARROW waveguide

Since light propagates through the core by total internal reflection at the air/core boundary, electric fields should be evanescent that is, exponentially decaying as x approaches $+\infty$. Besides, the mode in the core is a standing wave with a node at the interface between the core and the first high-index reflector layer, and exponentially decaying to zero amplitude just outside the low-index boundary.

Thus, the fields can be formulated in the following forms:

$$E_y(x) = \begin{Bmatrix} B_1 \exp(-k_1 x) \\ B_1 (\cos(k_2 x) - (k_1/k_2)\sin(k_2 x)) \\ B_2 \cos(k_3 x) - B_3 (k_2/k_3) \sin(k_3 x) \\ (B_4/k_3) \cos(k_2 x) - (B_5/k_2) \sin(k_2 x) \end{Bmatrix} \begin{matrix} x \geq d \\ o \leq x \leq d \\ -t_1 \leq x \leq 0 \\ x \leq -t_1 \end{matrix} \qquad (2.7)$$

The constants k_1, k_2, k_3, k_4 are the transverse propagation constants in air, core, first cladding and substrate respectively. They are obtained from the dispersion relations in the core and surrounding dielectric regions, that is, applying equation (2.6) to (2.7) results in

$$\begin{aligned} k_1 &= \sqrt{k_z^2 - k_0^2 n_0^2} \\ k_2 &= \sqrt{k_0^2 n_c^2 - k_z^2} \\ k_3 &= \sqrt{k_0^2 n_1^2 - k_z^2} \\ k_4 &= \sqrt{k_0^2 n_s^2 - k_z^2} \end{aligned} \qquad (2.8)$$

where

k_0 is the propagation factor in free space (μm^{-1})

n_c is the refractive index in the core

n_0 is the refractive in the air

n_1 is the refractive index in the first cladding layer

n_s is the refractive index in the substrate

k_z is the propagation factor of ARROW waveguide (μm^{-1})

By matching the tangential fields in the boundary layers, the coefficients (B_2, B_3, B_4 & B_5 are found:

$$\begin{aligned} B_2 &= \cos(k_2 d) + (k_1/k_2) \sin(k_2 d) \\ B_3 &= \sin(k_2 d) - (k_1/k_2) \cos(k_2 d) \\ B_4 &= k_3 B_2 \cos(k_3 t_1) + k_2 B_3 \sin(k_3 t_1) \\ B_5 &= k_2 B_3 \cos(k_3 t_1) - k_3 B_2 \sin(k_3 t_1) \end{aligned} \qquad (2.9)$$

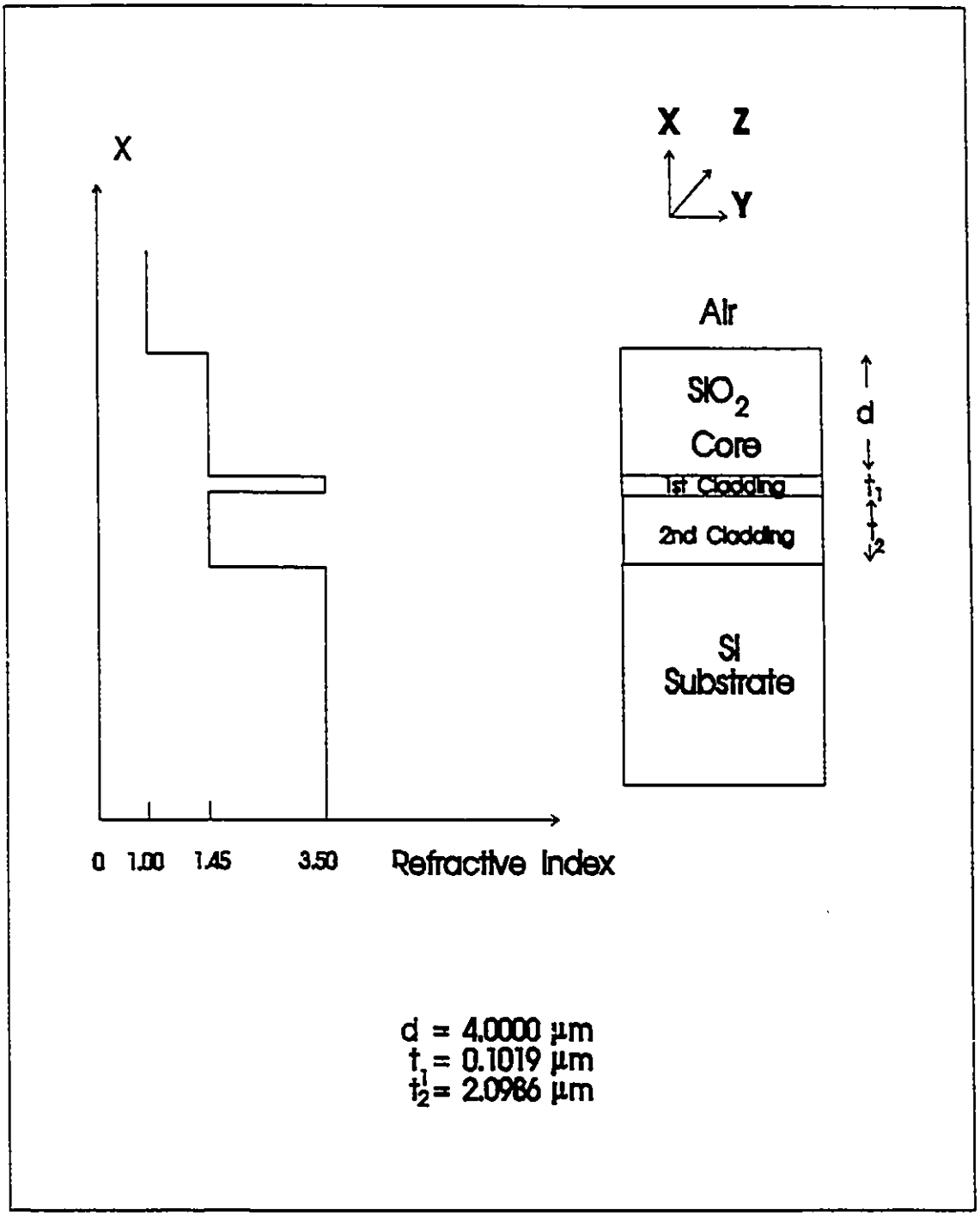

Fig.2.4: Optimum Dimensions of a Planar ARROW Waveguide

The light intensity $|E_y|^2$ of TE fundamental mode as a function of distance into the substrate is plotted in Fig.2.5 which shows the intensity profile in the guided mode when equations (2.4) and (2.5) are satisfied. The TE mode field is confined strongly inside the core and little light radiates to the substrate.

2.3 The Effective Refractive Index of an ARROW Waveguide

Before defining the effective refractive index, let us review some basic optical laws and definitions. Light consists of an electric and a magnetic field that oscillate at very high rates, on the order of 10^{14} hertz. The electric field travelling in the z-direction can be written as

$$E = E_0 \sin(\omega t - kz) \tag{2.10}$$

where E_0 is the peak amplitude

ω is the radian frequency.

The term k is the propagation factor.

It is given by

$$k = \frac{\omega}{V} \tag{2.11}$$

where

V is the wave velocity (m/s).

In free space a light wave travels at a speed $c=3\times10^8$ m/s. The speed of light is the product of the frequency and the wavelength. Upon entering a dielectric medium the wave now travels at a velocity V, which is characteristic of the material and less than c. The ratio of the speed of light in a vacuum to that in matter is the index of refraction n_c of the material and is given by

$$n_c = \frac{c}{V} \tag{2.12}$$

Combining equation (2.11) and (2.12), the propagation factor can be written as

$$k = \frac{\omega n_c}{c} \tag{2.13}$$

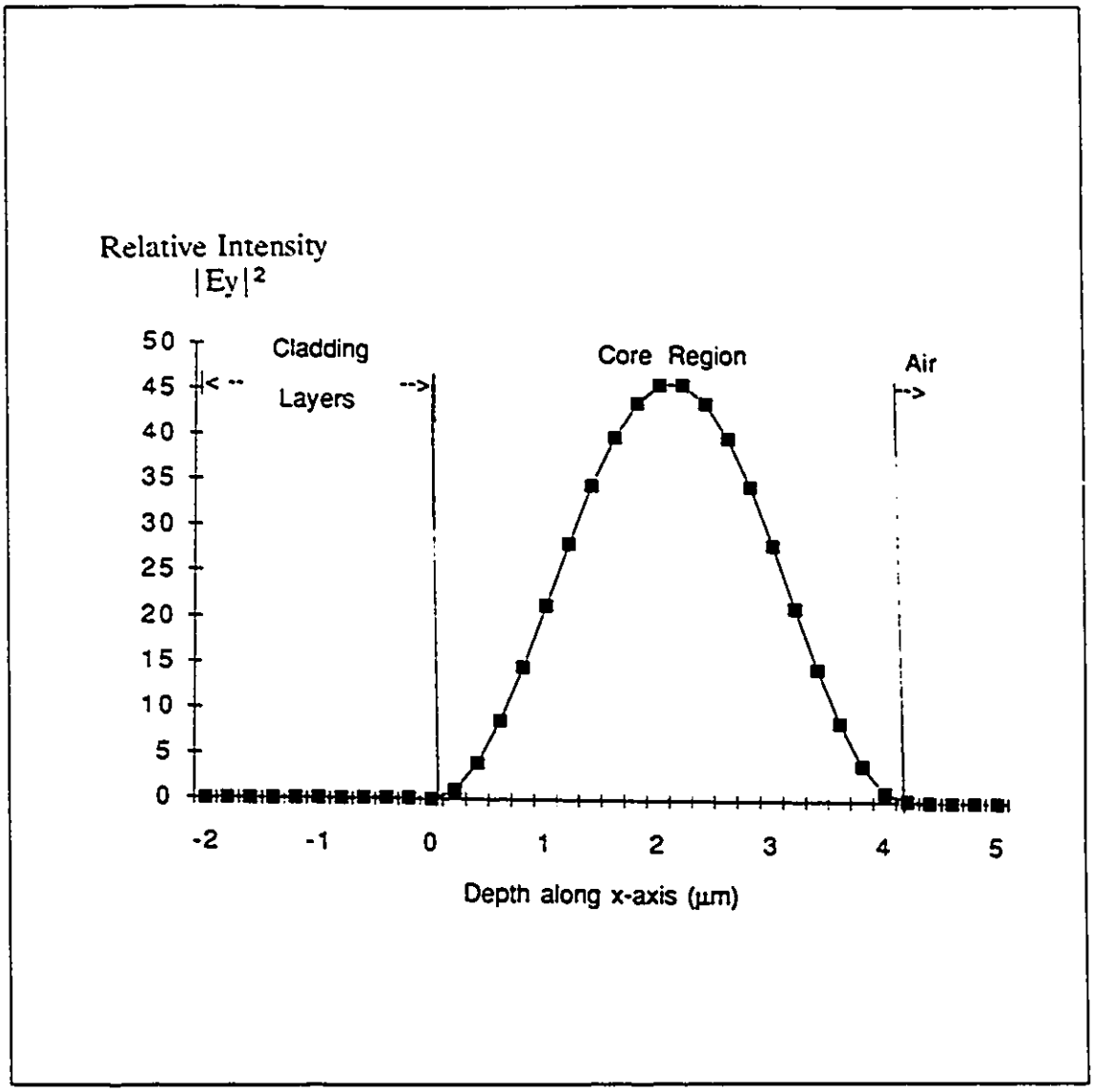

Fig.2.5: Light intensity of TE_0 Mode as a Function of Distance into the Substrate

The propagation factor in free space can be denoted by k_0. Since n=1 in free space,

$$k_0 = \frac{\omega}{c} \tag{2.14}$$

Combining equation (2.13) and (2.14), the propagation constant in any medium can be described in terms of the free-space propagation value by

$$k = k_o n_c \tag{2.15}$$

The TE fundamental mode in the core of an ARROW waveguide propagates as a plane wave which goes in a zigzag, back and forth at the incident angle ξ. We can consider the total field as the sum of two uniform plane waves, one travelling forward and the other travelling backward. The propagation constant is drawn in Fig.2.6. The component of the propagation factor along the z direction (propagation factor) is

$$k_z = k\cos\xi_c = k_0 n_c \cos\xi_c \tag{2.16}$$

where k_z is the longitudinal propagation constant

Comparison with equation (2.10) for an unguided wave shows the same variation along the direction of travel, except for the replacement of k by k_z. By making this replacement in equation (2.11), the waveguide wave velocity V_g and the longitudinal propagation constant can be related as

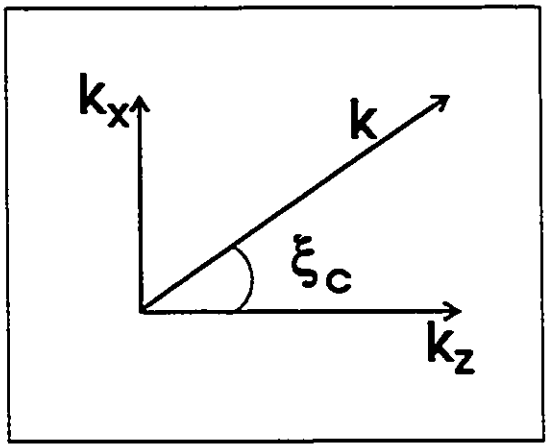

Fig.2.6: Propagation Constant of Wave in an ARROW Waveguide

$$k_z = \frac{\omega}{V_g} \tag{2.17}$$

The refractive index is defined as the velocity of light in free space divided by the velocity in an unbounded medium. Similarly, effective refractive index (n_{eff}) can be defined as the free-space velocity divided by the

guided velocity (V_g). That is, $n_{eff} = c/V_g$. Then, using equations (2.9) and (2.12), we obtain

$$n_{eff} = \frac{ck_z}{\omega} = \frac{k_z}{k_0} \tag{2.18}$$

The effective refractive index (n_{eff}) is a key parameter in guided propagation, just like the refractive index in unguided propagation. The effective refractive index concept has applications to approximate a 3-dimensional waveguide by a 2-dimensional one with an effective index profile derivable from the geometry and the refractive index profile of the original structure. In Chapter 3 we will see how to apply this effective refractive index to analyze 3-dimensional ARROW waveguide.

2.3.1 Determination of Effective Index based on Geometric Optics

Recall equation (2.16),

$$k_z = k_0 n_c \cos\xi_c \tag{2.19}$$

Besides, the effective index is defined as

$$n_{eff} = \frac{k_z}{k_0} = n_c \cos\xi_c \tag{2.20}$$

Recall equation (2.2),

$$\sin\xi_c \approx \frac{\lambda}{2n_c d_e} \tag{2.21}$$

Note that equation (2.21) is independent of n_1 or n_2 of the cladding layers. Thus, the effective refractive index can be expressed as follows:

$$n_{eff} = k_0 n_c \left[1 - \left(\frac{\lambda}{2n_c d_e}\right) \right]^{\frac{1}{2}} \tag{2.22}$$

where

d_e is the equivalent core thickness due Goos-Häenchen shift [16] as shown in Fig.2.3, which is the lateral shift of a light ray at the core/air or core/cladding boundaries.

2.3.2 Determination of Effective Index based on Electromagnetic Theory

ARROW waveguide analysis based on electromagnetic theory instead of ray analysis is given in [17]. The equivalent transmission-line and transverse resonance method are used to derive the dispersion equation of an ARROW waveguide [17] as shown in Fig.2.7. Y_m and γ_m are the characteristic admittance and complex transverse propagation in the m-th layer, respectively. According to transmission line theory [6], the input admittance at the 2nd cladding/substrate layer boundary looking downward, $Y_{in,3}$, is

$$Y_{in,3} = Y_3 \frac{Y_{lb} + Y_3 \tanh(\gamma_3 l)}{Y_3 + Y_{lb} \tanh(\gamma_3 l)} \tag{2.23}$$

where

Y_{lb} is the load admittance

Y_3 is the characteristic admittance of the substrate

l is the substrate thickness as shown in Fig.2.7.

γ_3 is the complex transverse propagation factor in the Si substrate

If the substrate is thick enough compared to the wavelength of light ($l >> \lambda$), $\tanh(\gamma l) \rightarrow 1$. Therefore, Y_{in3} becomes progressively less dependent on load admittance or $Y_{in,3} \approx Y_3$. Similarly, the input admittance at the air/core interface looking upward, $Y_{in,a}$ can be approximated as $Y_{in,a} \approx Y_a$

Considering the core/1st cladding boundary as in Fig.2.7, the sum of input admittances is zero. Therefore, the transverse resonance condition is

$$Y_{in,c} + Y_{in,1} = 0 \tag{2.24}$$

where at the core/1st cladding layer interface, $Y_{in,c}$ is the input admittance looking upward and $Y_{in,1}$ is the input admittance looking downward .

The dispersion equation for TE_0 of an ARROW Waveguide is given by [17] as follows:

$$\gamma_c \frac{\gamma_a + \gamma_c \tanh(\gamma_c d)}{\gamma_c + \gamma_a \tanh(\gamma_c d)} = \gamma_1 \frac{\overline{Y_{in,2}} + \gamma_1 \tanh(\gamma_1 t_1)}{\gamma_1 + \overline{Y_{in,2}} \tanh(\gamma_1 t_1)} \tag{2.25}$$

where

$$\overline{Y_{in,2}} = \gamma_2 \frac{\gamma_3 + \gamma_2 \tanh(\gamma_2 t_2)}{\gamma_2 + \gamma_3 \tanh(\gamma_2 t_2)} \tag{2.26}$$

The dispersion equation (2.25) applies to an ARROW waveguide without the cladding layers being optimum for anti-resonance or not. After solving the dispersion equation, the effective refractive index (n_{eff}) can be determined. If the ARROW waveguide is under optimum condition for minimum loss, the Febry-Perot interferometer is under anti-resonance. That means both $\gamma_1 t_1$ and $\gamma_2 t_2$ equal $\pi/2$. As a result, (2.25) can be greatly simplified as follow:

$$\kappa_c + \alpha_a \tan(\kappa_c d) = 0 \tag{2.27}$$

where κ_c is the imaginary part of the transverse propagation in the core

α_a is the real part of the transverse propagation in air

The derivation of equations (2.25) and (2.27) are given in Appendix E.

2.3.3 Comparison of the Effective Index from Section (2.3.1) and (2.3.2)

The exact and approximate solutions of effective index for the TE_0 mode versus the variation of core thickness.d, are shown in Fig.2.8 with t_1 = 0.1019 μm and t_2 = 2.0985 μm for an optimum structure of d=4.0 μm at λ=1.3 μm as derived from equations (2.4) and (2.5). When d = 4 μm, the effective index is calculated as 1.441709 and 1.440866 for equation (2.27) and equation (2.22), respectively. Since the solution from electromagnetic theory analysis, i.e. equation (2.27), is more accurate than the one from geometric optics analysis, equation (2.22), effective index n_{eff} is taken as 1.441709 with t_1(Si) = 0.1019 μm and t_2(SiO_2) = 2.0985 μm for an optimum structure of d=4.0 μm at

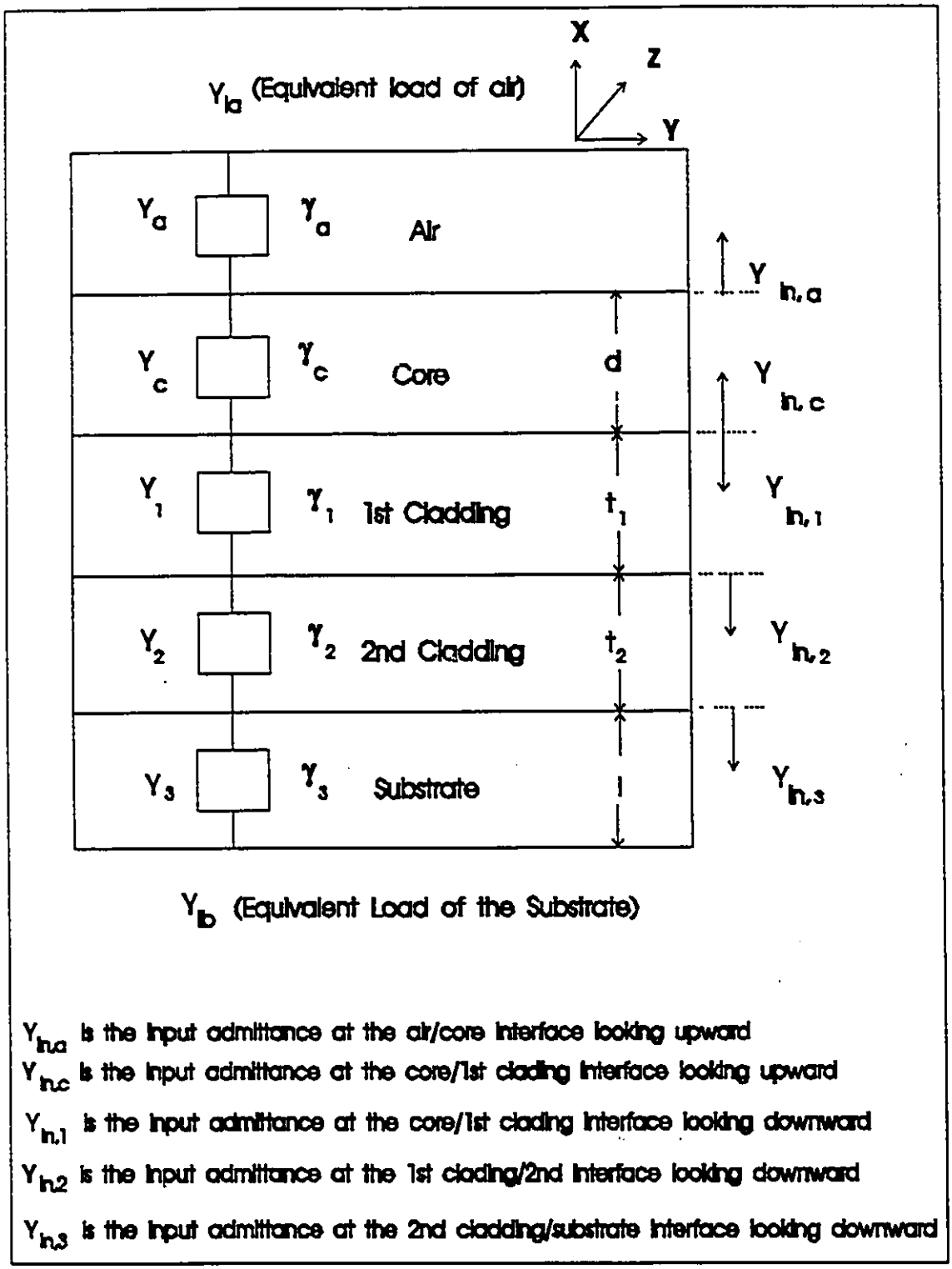

Fig.2.7: Transmission Line Equivalent Circuit of an ARROW Waveguide

λ=1.3 μm.

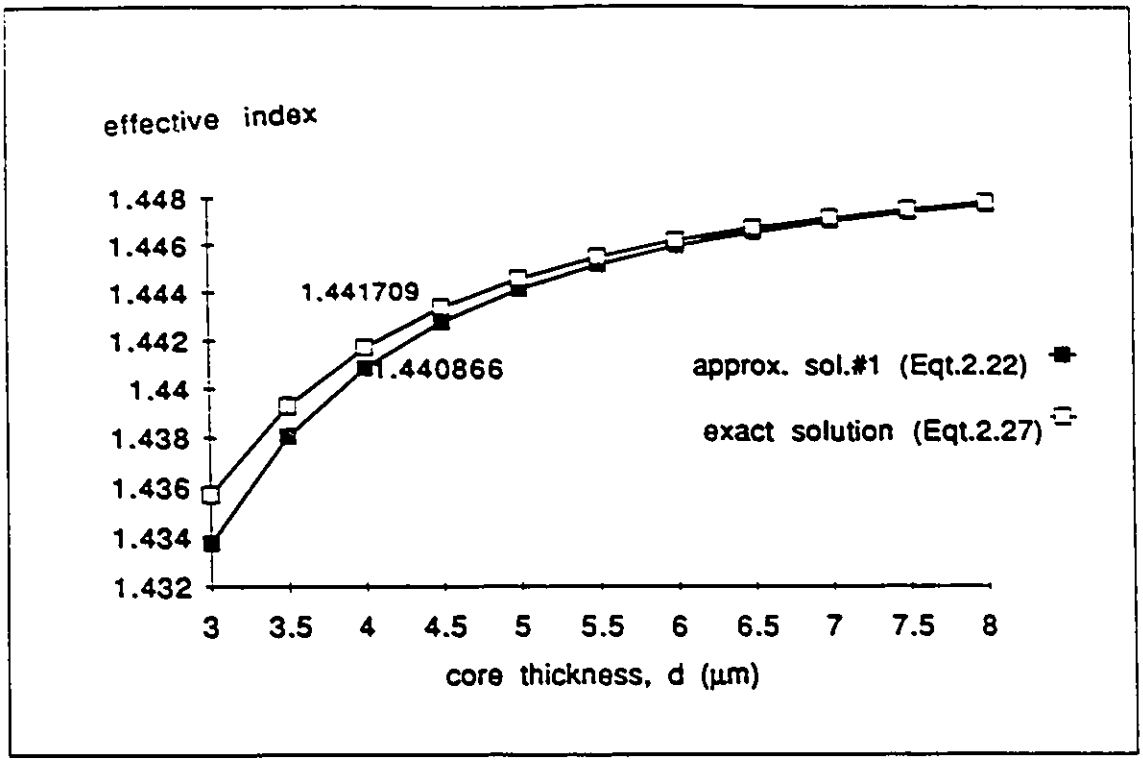

Fig.2.8: The Effective Index of the ARROW Waveguide (the Cladding Layers are Optimum for 4 μm Core)

2.4 Propagation Loss in an ARROW Waveguide

In an ARROW waveguide, the reflectivity from the interface cladding is produced by the sum of simple Fresnel reflections at the boundaries between the core, the cladding layers and the substrate. Therefore, the loss of the TM mode is much larger than that of the TE modes due to the difference between the reflectivities for the two polarizations. Although low-loss operation of an ARROW waveguide relies upon properly phased reflections from all the interfaces, the wave in the ARROW waveguide will propagate within a wide band of frequencies. It is because the resonant frequencies of a Fabry-Perot interferometer

occur over a narrow band and the antiresonant frequencies are spectrally broad.

The expression of the loss coefficient of the TE_0 mode has been formulated [16]. Also, [16] expressed the loss constant in terms of the power reflectivities of interface cladding layer for the fundamental mode as:

$$\alpha_0 = 2.17\ (1-R)\ \frac{\tan\xi_c}{d_e} \qquad \text{dB/m} \qquad (2.28)$$

where R is the power reflectivity of interference cladding layer

ξ is the incident glancing angle

d_e is the equivalent core thickness

The derivation of equation (2.28) is given in Appendix F

After expressing the power in terms of the refractive indexes of different layers, the loss coefficient of the fundamental mode under optimum conditions is

$$\alpha_0 = \frac{86859\lambda^4\ [\ (n_1^2-n_c^2) + (\frac{\lambda d_e}{2})^2\ ]^{-1}}{n_c d_e^5\ [1-(\frac{\lambda}{2}n_c d_e)^2\ ]^{\frac{1}{2}}\ [\ (n_s^2-n_c^2) + (\frac{\lambda}{2}d_e)^2\ ]^{\frac{1}{2}}} \qquad \text{dB/m} \qquad (2.29)$$

where λ is the wavelength (μm)

n_c is the refractive index in the core

n_1 is the refractive index in the first cladding

n_s is the refractive index in the substrate

The derivation of equation (2.29) is given in Appendix G.

From equation (2.29) the loss constant, α_0, depends on λ and d_e. If d_e is increased and λ is decreased, the propagation loss, α_0 will be smaller.

2.5 Advantages of ARROW Waveguides over Conventional Waveguides

In the ARROW waveguide structure, the ARROW waveguide mode is confined at the upper surface (air) by conventional total internal reflection, but on the other substrate side

by phased reflections from the interfaces of two higher-index reflector layers. These layers and the intervening space form a series of Fabry-Perot resonators all in anti-resonance for spectrally broad bandwidth. Because of the above structure, the ARROW waveguide shows great promise for a single-mode optical coupler based on the following reasons:

1) They show a lower loss in broad wavelength range (<0.4 dB/cm) than conventional waveguides.

2) The TE fundamental mode propagates by the filtering of high order modes due to loss discrimination associated with the propagation.

3) Fabrication is easier because precise control of the refractive indexes is not necessary to achieve anti-resonance.

4) Conventional optical slab waveguides need a thick cladding for reducing the decaying evanescent field in air, whereas only thin cladding (~ 2 μm for a 4 μm core) is needed for large light confinement in the ARROW waveguide.

5) They have a high potential for integration with other optical and electronic devices on a single chip since they are all formed on a Si substrate.

6) The coupling efficiency between ARROW waveguide ribs and optical fibres can be very high if the ribs are well designed.

Chapter 3

Effective Index Method

3.1 Introduction

The slab ARROW waveguide analyzed in the last chapter is an accurate representation of single direction guiding because of the infinite spatial extent of the wave in the Y-direction as shown in Fig.2.2. An important feature of optical integrated circuit waveguides is the capability to confine optical energy in both transverse directions (both X and Y-direction). The waveguides are referred to as three-dimensional structure when light confinement occurs in both transverse directions. A number of three-dimensional waveguide structures exist including strip optical waveguide, insulated image waveguides and strip-slab waveguides. Different types of three-dimensional waveguide geometries have been successfully analyzed by various methods [18], among which the finite element method [19]-[21], the point-matching method and the effective index method are typical ones. The effective index method was initially proposed [22] for the analysis of rectangular-core dielectric waveguides as a modification of Marcatili's method [23]. The generic feature of the effective index has been extended to account for other waveguide structures [24]-[26]. The central idea of the method is to replace the optical waveguide by an equivalent slab waveguide whose refractive index profile is determined from the geometrical shape of the waveguide. The success of converting the three-dimensional problem to a two-dimensional problem makes the method significantly more efficient and simpler than other methods.

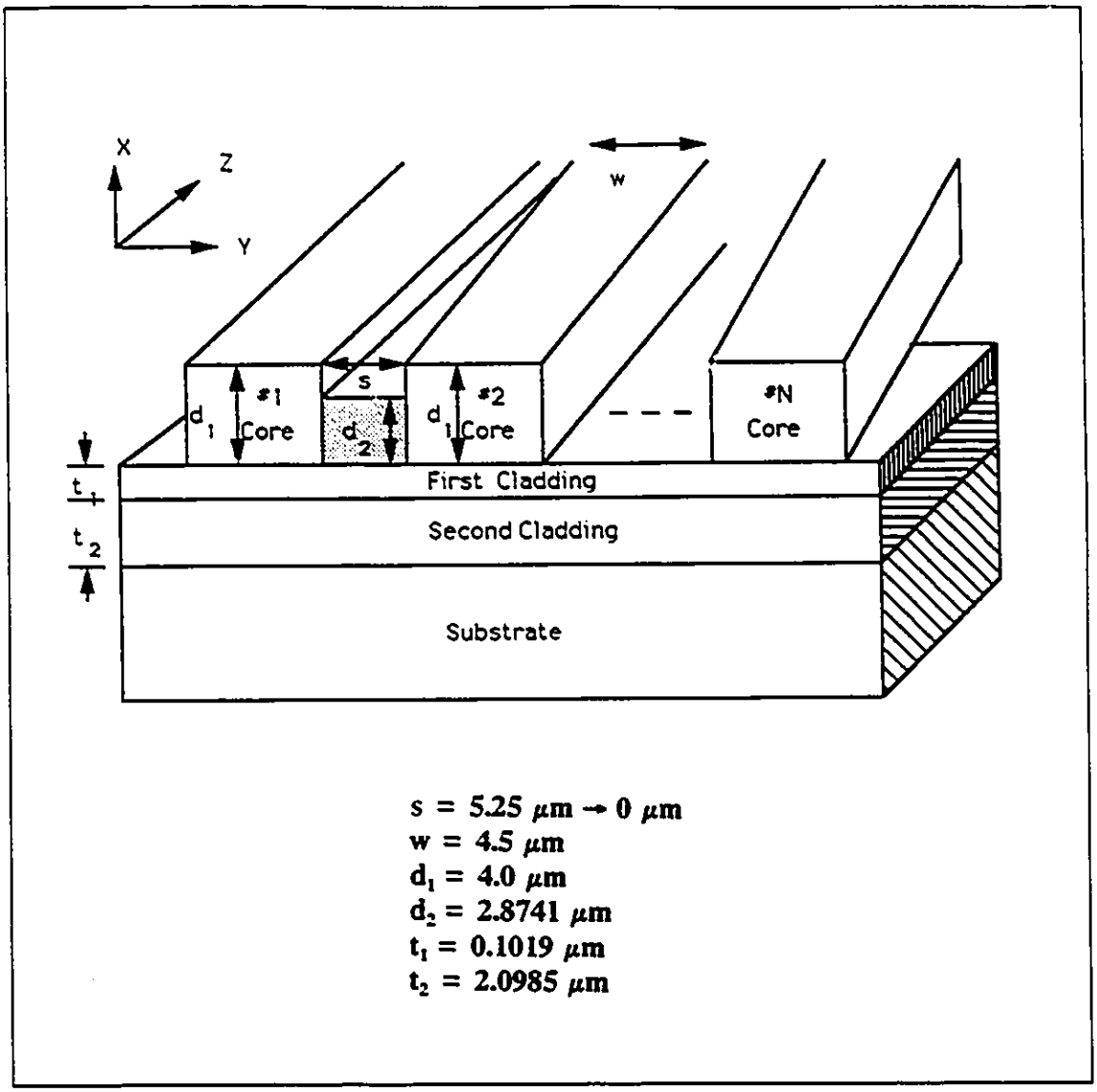

Fig.3.1: 3-Dimensional Coupled ARROW Waveguide

3.2 Effective Index Method in ARROW Waveguide

Let us analyze the ARROW 3-D waveguide shown in Fig.3.1. The detailed structure has been given in the previous chapter. The core is made of SiO_2. The core bounded on the upper surface by a low-index medium (air) to produce total internal reflection, but bounded on the lower surface by an interference cladding which is composed of high index layer (1st cladding), Si layer and low index (2nd cladding), SiO_2 layer. Thus, light propagates through the core by repeating total internal reflection at the upper air/SiO_2 boundary and extremely high reflection from the interference cladding when the thicknesses of the interference cladding layers satisfy the anti-resonant condition. For anti-resonant condition, maximum reflection occurs in the cladding layers i.e. most of the light energy is reflected back to the core region. Slab ARROW waveguide is analyzed in the xy plane as shown in Fig.3.2. If the waveguide structure is viewed in the yz plane, as shown in Fig.3.3 , then the structure appears equal to that of an asymmetric slab waveguide having a guiding region with refractive index n_{eff1} and n_{eff2} with space s, and width w, as shown in Fig.3.3. Note that n_{eff2} is the core layer and n_{eff1} is the cladding layer in the yz plane. Referring to Fig.3.2, n_{eff1} (1.441709) is the effective index of the ARROW with d_1 = 4 μm and n_{eff2} (1.434455) is the effective index with d_2 = 2.8741 μm. n_{eff2} is chosen to be 1.434455 so that only the fundamental mode can exist in the yz plane. The effective refractive index may be interpreted as that of a hypothetical medium in which the propagation constant is equal to that of the original structure. The effective refractive index has been described in the previous chapter. Having determined the effective refractive index of the various regions, the guide in Fig.3.1 can be analyzed by modelling it with the 2n+1 layered structure. The steps in applying the effective index method to the coupler are shown in Fig.3.2 and Fig.3.3.

The propagation constant in the slab of core thickness, d_1 is first calculated and use to define an effective index n_{eff1}, which forms the refractive index of n parallel identical slabs of thickness w, separated by s which varies from 5.25 μm to zero as shown in Fig.3.1. The propagation constant of the composite waveguide formed by array of slabs is then used to approximate the propagation constant of the original three-dimensional

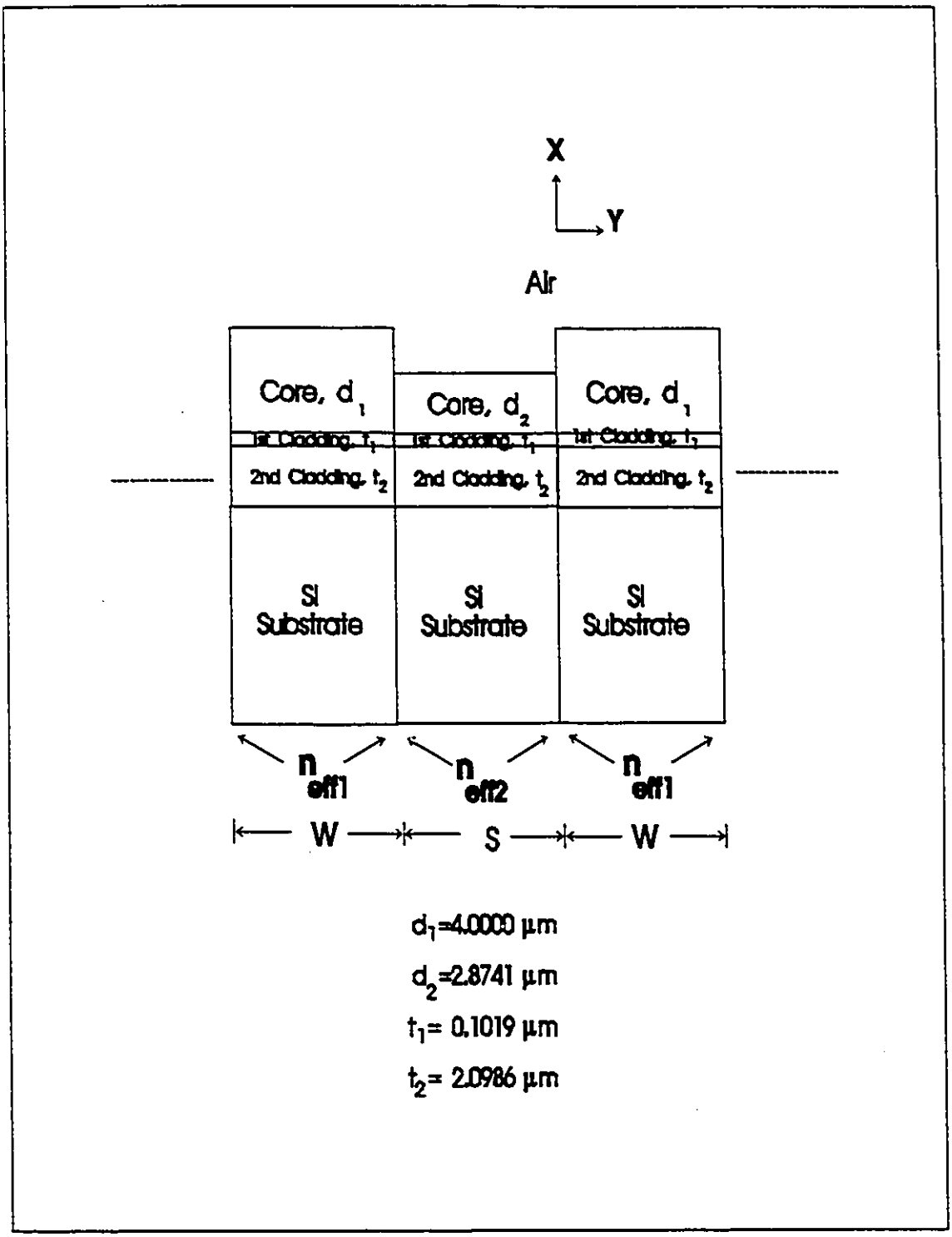

Fig.3.2: Structure for Analysing X-Variation in 5-Layer ARROW Waveguide

coupler. The propagation constant β for the original 5-waveguide structure is determined by matching the tangential fields on the boundaries. The individual steps in this method of analysis will be discussed in detail in the next chapter.

3.3 Conclusions:

The effective index method is a widely adopted approximation technique to determine propagation constants and field distributions of fundamental modes of dielectric waveguides. The method of analysis, based on the concept of effective index, have been shown to be an excellent approach to the study of certain types of optical waveguides [28]-[30]. However, this approach is still an approximate technique. It can be expected the approach will work well, only for:

i) Large aspect ratios (w/t > 1) [18].

ii) The operating frequency is far from cut-off frequency [28].

iii) The difference between the relative refractive indices involved is small [27].

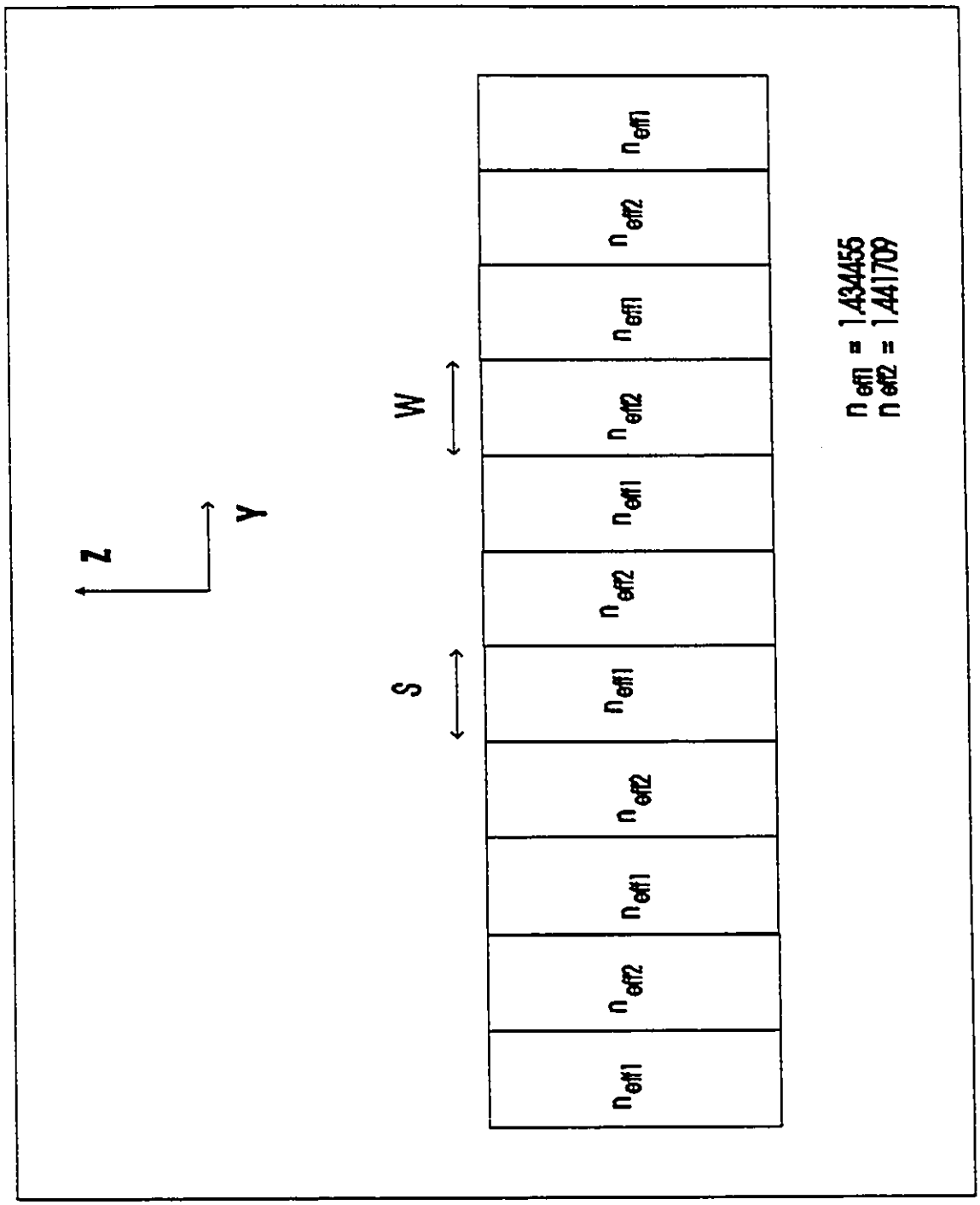

Fig.3.3: Structure for Analysing Y-Variation Using Concept of Effective Index Method

Chapter 4

NXN Passive Optical Star Coupler in Planar Waveguide

4.1 Introduction

Passive star couplers are needed in high-capacity local-area networks to accept signals from all transmitters and broadcast these to all receivers which can access the messages in the network and select one.

Each input waveguide can only support a single mode by making the refractive index in the separation (n_{efl}) close to the one in the waveguide (n_{eff2}) [31].

There are four different regions in the couplers as shown in Fig.4.1 [32]. The uncoupled region is used to allow input signal from the optical fibre to couple to the device without any influence from its neighbours. In the transition region, the input waveguides merge into a single waveguide slowly to allow the input signal to illuminate the transmitting aperture no matter which input waveguide is excited. After diffraction, the illuminated receiving waveguide is branched into N waveguides. Each output waveguide is supposed to carry the same power if the index symmetry is valid.

4.2 Scalar Wave Equation in Planar Waveguide

The spatial dependence of the electric field E(x,y,z) and the magnetic field H(x,y,z) of

an optical waveguide is determined by Maxwell's equations. The dielectric constant $\varepsilon(x,y,z)$ can be related to the refractive index $n(x,y,z)$ of the waveguide by $\varepsilon=n^2\varepsilon_o$, where ε_o is the dielectric constant of air. Under these conditions, Maxwell's equations for a

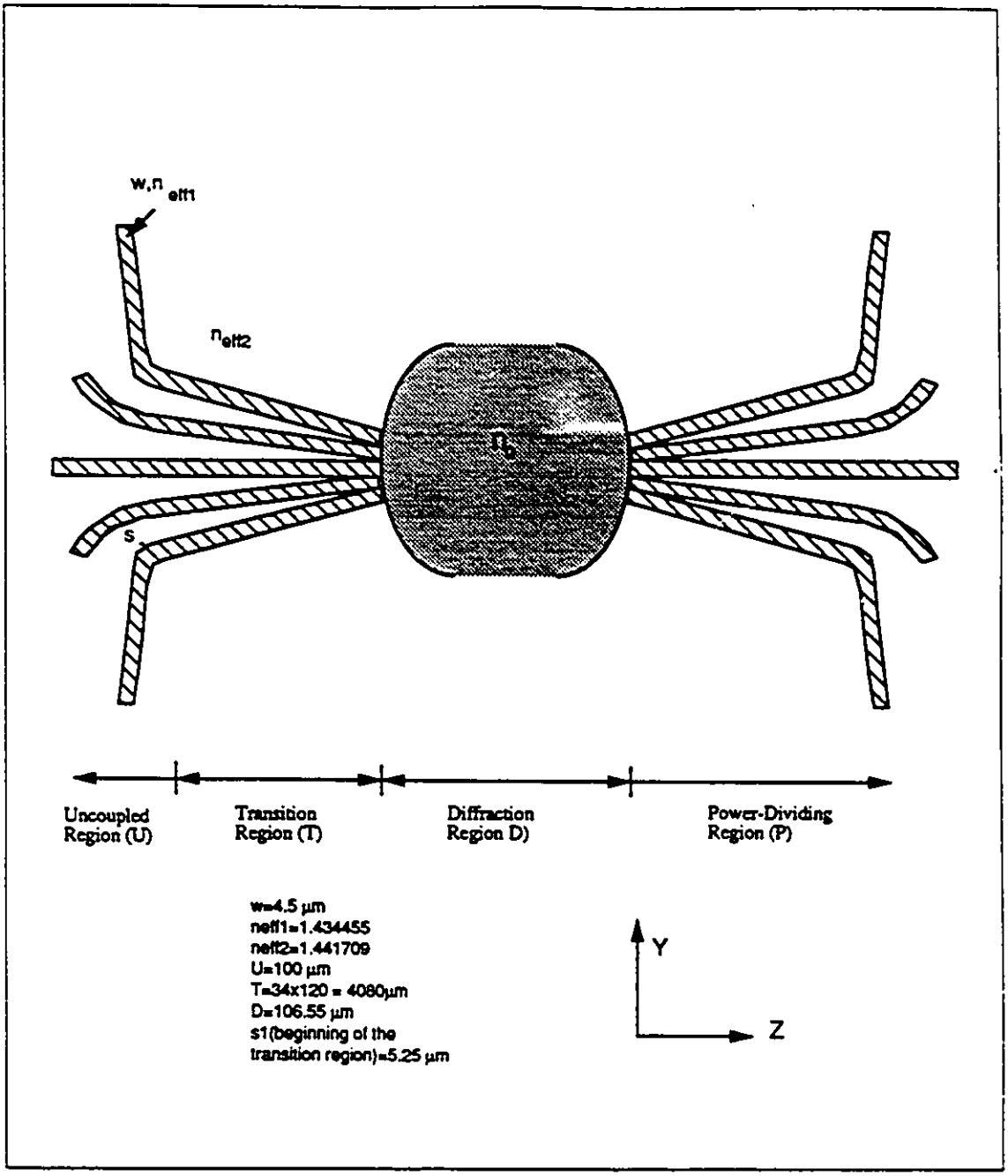

Fig.4.1: The Four Regions in the Planar Star Coupler

source-free, anisotropic medium are expressed as [6]:

$$\nabla \times E = -j(\mu_o/\varepsilon_o)^{1/2} kH \; ; \quad \nabla \times H = j(\mu_o/\varepsilon_o)^{-1/2} kn^2 E$$
$$\nabla \cdot n^2 \cdot E = 0 \qquad ; \nabla \cdot H = 0 \tag{4.1}$$

where k = $2\pi/\lambda$ is the free-space wavelength

λ = is the wavelength of light in free space

ε_o is the free space dielectric constant

μ_o is the free space permeability

After taking ∇x of the above equation and eliminating either H or E, the following vector wave equation for the cartesian components of the fields is obtained.

$$\nabla^2 E + k^2 n^2 \cdot E = \nabla(\nabla \cdot E)$$
$$\nabla^2 H + k^2 n^2 H = -j(\mu_o/\varepsilon_o)^{-1/2} k(\nabla n^2 \times E) \tag{4.2}$$

From section 2.2.1, the electric field component E_y of the TE mode is the only electric field component. Besides, in a planar waveguide with refractive index profile is $n = n(y)$. Therefore $\nabla n^2 \times E$ of equation (4.2) is identical to zero.

If it is true, equation (4.2) becomes

$$\nabla^2 H + k^2 n^2 H = 0 \tag{4.3}$$

In a planar waveguide with refractive index profile n(y), the magnetic field is as follows:

$$H(x,y,z) = H(y)\exp(-j\beta z) \tag{4.4}$$

If we use the representation of equation (4.4) and substitute into equation (4.3), we obtain

$$\frac{\partial}{\partial y^2} H(y) + [n^2(y)k_0^2 - \beta^2]H(y) = 0 \tag{4.5}$$

Thus, the magnetic fields of the TE modes obey the scalar wave equation.

4.3 Uncoupled region

The purpose of this region is to let input optical fibres couple to the input waveguides without electromagnetic interaction with adjacent waveguides. Thus, a signal entering any one of the waveguides is initially unaffected by the presence of the other waveguides due

to the large separation (200 μm). All the input waveguides have the same width, w and index, n_{core}. Meanwhile, the separation is varying in width with constant index, n_{em}. Different coupled-mode theories exist [33,34]. Our approach is to obtain the exact solution for the transverse normal modes from the scalar wave equation [10]. Recall equation (4.5),

$$\frac{\partial}{\partial y^2}H(y)+[n^2(y)k_0^2-\beta^2]H(y)=0 \tag{4.6}$$

Recall equation (4.4), the eigen solution should be in the form:

$$H(x,y,z) = H(y)\exp(-j\beta z) \tag{4.7}$$

where β is the propagation constant in the z-direction

4.3.1 Normal Modes of the N-waveguide Array

According to [22], the exact eigenmode theory gives the best accuracy as compared to other coupling theory. The magnetic field distribution in the various layers of N waveguides is given [23]. For the sake of clarity, a 5-input waveguide is used as an illustration for solving the scalar wave equation of the general N-input waveguide system as shown in Fig.4.2.

By making use of the fact that the fields are either symmetric or anti-symmetric in the symmetric system, the fields of the 5 waveguides in various layers (H_x) can be obtained as follows:

$H_1 = A_1 \exp(k_{1y} y)$ $\quad y \le y_1$

$H_2 = A_2 \cos(k_{2y} y) + B_2 \sin(k_{2y} y)$ $\quad y_1 \le y \le y_2$

$H_3 = A_3 \cosh(k_{1y} y) + B_3 \sinh(k_{1y} y)$ $\quad y_2 \le y \le y_3$

$H_4 = A_4 \cos(k_{2y} y) + B_4 \sin(k_{2y} y)$ $\quad y_3 \le y \le y_4$

.

.

$H_{11} = A_{11} \exp(-k_{1y} y)$ $\quad y \ge y_{10}$

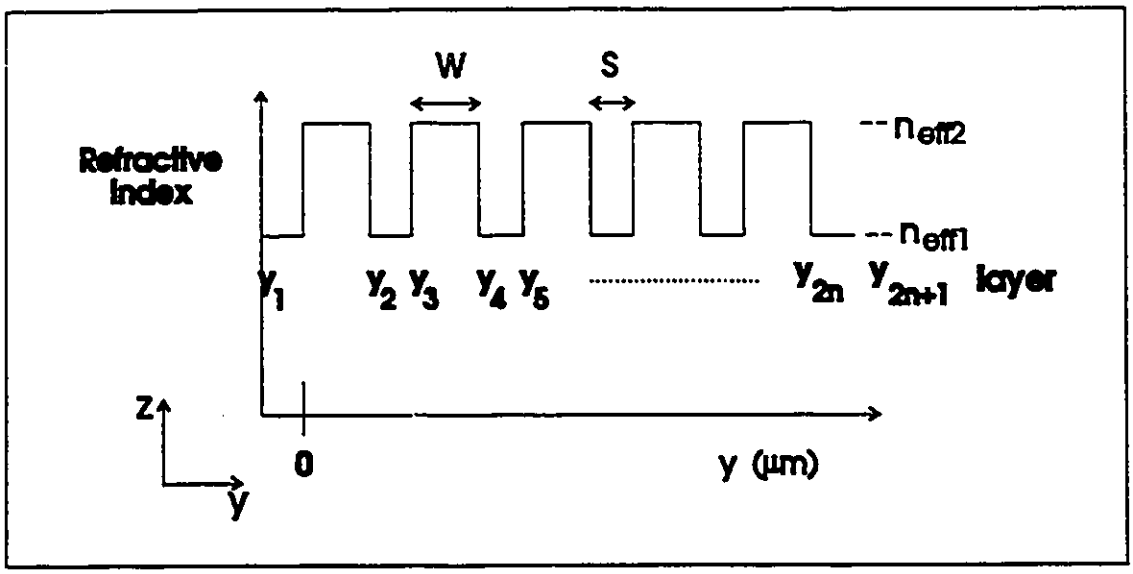

Fig.4.2: Schematic Cross Section of a 5-Waveguide Coupler

where H_i represents the field in the i_{th} layer

$y_1 = 0$

$y_2 = w$

$y_3 = w+s$

$y_4 = 2w+s$

.

.

$y_{10} = 4(w+s)$

The constant k_{1y}, k_{2y} are real and given by

$$k_{1y}=\sqrt{\beta^2-n_{eff2}^2k_0^2} \tag{4.8}$$

$$k_{2y}=\sqrt{n_{eff1}^2k_0^2-\beta^2} \tag{4.9}$$

By matching the tangential fields in the boundary layers, the coefficients (A_i & B_i)

can be obtained in terms of the ones in the previous layer. Additional to this, the guidance condition can be formulated as:

$$\tan(k_2 w)=\left(\frac{k_2 B_{10}+k_1 A_{10}}{k_2 A_{10}-k_1 B_{10}}\right) \tag{4.10}$$

The derivation of equation (4.10) is given in Appendix H. Numerical methods have been used to solve this above transcendental equation. Considering the above equation, there will be 5 different solutions, k_{2y}. Each k_{2y} can contribute a solution. The 5 normal modes (A, B, C, D, E) under weak coupling are plotted in Fig.4.3. From [34], when the array has identical channels and uniform coupling, the relative magnetic field amplitude of the normal modes across the waveguide array can be approximated as:

$$H_l^{\nu}=\sin\left(l\frac{\pi\nu}{n+1}\right) \tag{4.11}$$

where $\nu = 1, 2, \cdots n$.

The relative magnetic field amplitudes ($H_{\nu l}$) have been summarised in Table 1. The concept can be applied to any number of waveguides. The relative fields among 7 waveguides are listed in Appendix I as an example.

ν (mode)	l=1	l=2	l=3	l=4	l=5
1 (A)	1.0	1.7321	2.0	1.7321	1.0
2 (B)	1.0	1.0	0.0	-1.0	-1.0
3 (C)	1.0	0.0	-1.0	0.0	1.0
4 (D)	1.0	-1.0	0.0	1.0	-1.0
5 (E)	1.0	-1.7321	2.0	-1.7321	1.0

Table 1: Relative Magnetic Field Amplitudes in Different Waveguides of the 5 Normal modes.

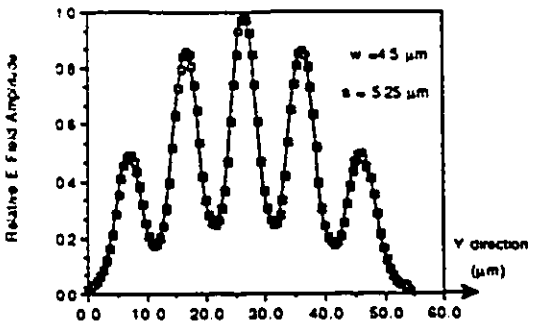

Fig 4.3a: Normal Mode A without Coupling

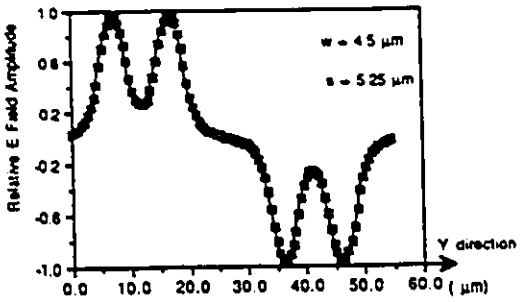

Fig.4.3b: Normal Mode B without Coupling

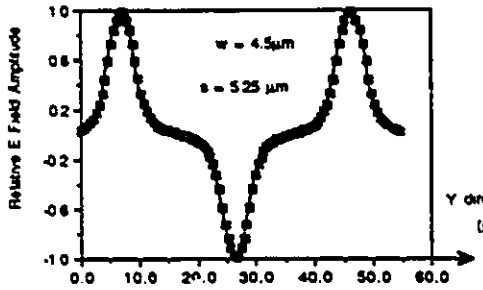

Fig 4.3c: Normal Mode C without Coupling

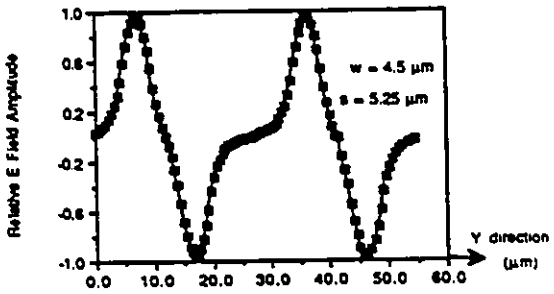

Fig 4.3d: Normal mode D without Coupling

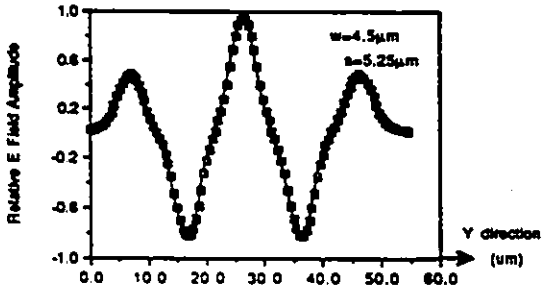

Fig 4.3e: Normal Mode E without Coupling

Fig.4.3: Magnetic Field Distribution of 5 Normal Modes of a 5-Waveguide Structure

Before any coupling between input waveguides, the field distribution across the waveguides can be expressed as a sum of the normal modes, with different weighting. Note that only lossless waveguides are assumed otherwise cross-coupling occurs. The initial field distribution without any coupling due to the i^{th} input waveguide on N waveguides is given as :

$$H^{i}(y,z=0)=\sum_{\nu=1}^{N}\sum_{l=1}^{N}\alpha_{il}H_{\nu l}(y) \qquad (4.12)$$

where

l = 1,2....N refers to one of the N waveguides in the structure

ν = 1,2..... refers to the one of the ν^{th}-order normal modes

i represents the waveguide number with input power signal

α_{il} is the weighting on $H_{\nu l}(y)$ of l^{th} waveguide [11].

For N=5, the coefficients α_{il} are given in Table 2. The determination of the weighting coefficient of the individual normal modes will be discussed in the next paragraph.

i	l=1	l=2	l=3	l=4	l=5
1	1.0	3.0	4.0	3.0	1.0
2	1.0	1.7321	0.0	-1.7321	-1.0
3	1.0	0.0	-2.0	0.0	1.0
4	1.0	-1.7321	0.0	1.7321	-1.0
5	1.0	-3.0	4.0	-3.0	1.0

Table 2: The Weighting Coefficient of the Normal Modes with Input to Different Waveguides

Note that the summation of the weighting coefficients is always zero with input to the even numbered waveguides.

4.3.2 Determination of the Weighting Coefficient of the Individual Normal Modes

For a N-input star coupler, the input power signal may come from any waveguide. It is easy to express the input waveguide in terms of normal modes as shown in Fig.4.3. To see how this model will work for various power waveguides, 3 cases will be examined for N=5. The idea can be applied to any N. Appendix J also gives the weighting coefficients for N=7.

4.3.2.1 Input Power Goes into the Centre Waveguide

When power only goes into the centre waveguide, only the A, C and E modes will be excited. Modes A and E will be excited such that they are subtractive in the second and the fourth waveguide and additive in the first, the third and the fifth waveguide. Mode C is excited so it is additive to the sum of modes A and E in the centre waveguide and subtractive in the first and fifth waveguide as shown in the following expressions.

$$(A_1, A_2, A_3, A_4, A_5, A_6) + (E_1, E_2, E_3, E_4, E_5) - 2(C_1, C_2, C_3, C_4, C_5)$$

$$=1(1, \sqrt{3}, 2, \sqrt{3}, 1) + 1(1, -\sqrt{3}, 2, -\sqrt{3},1) -2(1, 0, -1, 0, 1) = (0, 0, 6, 0, 0)$$

4.3.2.2 Input Power Goes into the First or the Fifth Waveguide.

i) The first waveguide has the input power.

All five normal modes will be excited in this case. The normal modes will be excited as follows:

$$(A_1, A_2, A_3, A_4, A_5, A_6) + (E_1, E_2, E_3, E_4, E_5) + 4(C_1, C_2, C_3, C_4, C_5) + 3(B_1,B_2, B_3,B_4, B_5) + 3(D_1, D_2, D_3, D_4, D_5)$$

$$=1(1, \sqrt{3}, 2, \sqrt{3}, 1) + 1(1, -\sqrt{3}, 2, -\sqrt{3},1) +4 (1, 0, -1, 0, 1) +3(1, 1, 0, -1, -1) +3 (1, -1, 0, 1, -1)] = (12, 0, 0, 0, 0)$$

ii) The Fifth waveguide has the input power

All five normal modes will be excited in this case. The normal modes will be excited as follows:

$(A_1, A_2, A_3, A_4, A_5, A_6) + (E_1, E_2, E_3, E_4, E_5) + 4(C_1, C_2, C_3, C_4, C_5) - 3(B_1, B_2, B_3, B_4, B_5) - 3(D_1, D_2, D_3, D_4, D_5)$

$= \mathbf{1}(1, \sqrt{3}, 2, \sqrt{3}, 1) + \mathbf{1}(1, -\sqrt{3}, 2, -\sqrt{3}, 1) + \mathbf{4}(1, 0, -1, 0, 1) - \mathbf{3}(1, 1, 0, -1, -1) - \mathbf{3}(1, -1, 0, 1, -1) = (0, 0, 0, 0, 12)$

4.3.2.3 Input Power Goes Into the Second or the Fourth Waveguide.

i) The second waveguide has the input power.

Only the A,B,D and E modes will be excited in this case. The normal modes will be excited as follows:

$(A_1, A_2, A_3, A_4, A_5) - (E_1, E_2, E_3, E_4, E_5) + \sqrt{3}(B_1, B_2, B_3, B_4, B_5) - \sqrt{3}(D_1, D_2, D_3, D_4, D_5)$

$= \mathbf{1}(1, \sqrt{3}, 2, \sqrt{3}, 1) - \mathbf{1}(1, -\sqrt{3}, 2, -\sqrt{3}, 1) + \sqrt{3}(1, 1, 0, -1, -1) - \sqrt{3}(1, -1, 0, 1, -1) = (0, 4\sqrt{3}, 0, 0, 0)$

ii) The fourth waveguide has the input power

Only the A,B,D and E modes will be excited in this case. The normal modes will be excited as follows:

$(A_1, A_2, A_3, A_4, A_5) - (E_1, E_2, E_3, E_4, E_5) - \sqrt{3}(B_1, B_2, B_3, B_4, B_5) + \sqrt{3}(D_1, D_2, D_3, D_4, D_5)$

$= \mathbf{1}(1, \sqrt{3}, 2, \sqrt{3}, 1) - \mathbf{1}(1, -\sqrt{3}, 2, -\sqrt{3}, 1) - \sqrt{3}(1, 1, 0, -1, -1) + \sqrt{3}(1, -1, 0, 1, -1)$

$= (0, 0, 0, 4\sqrt{3}, 0)$

4.4 Transition Region

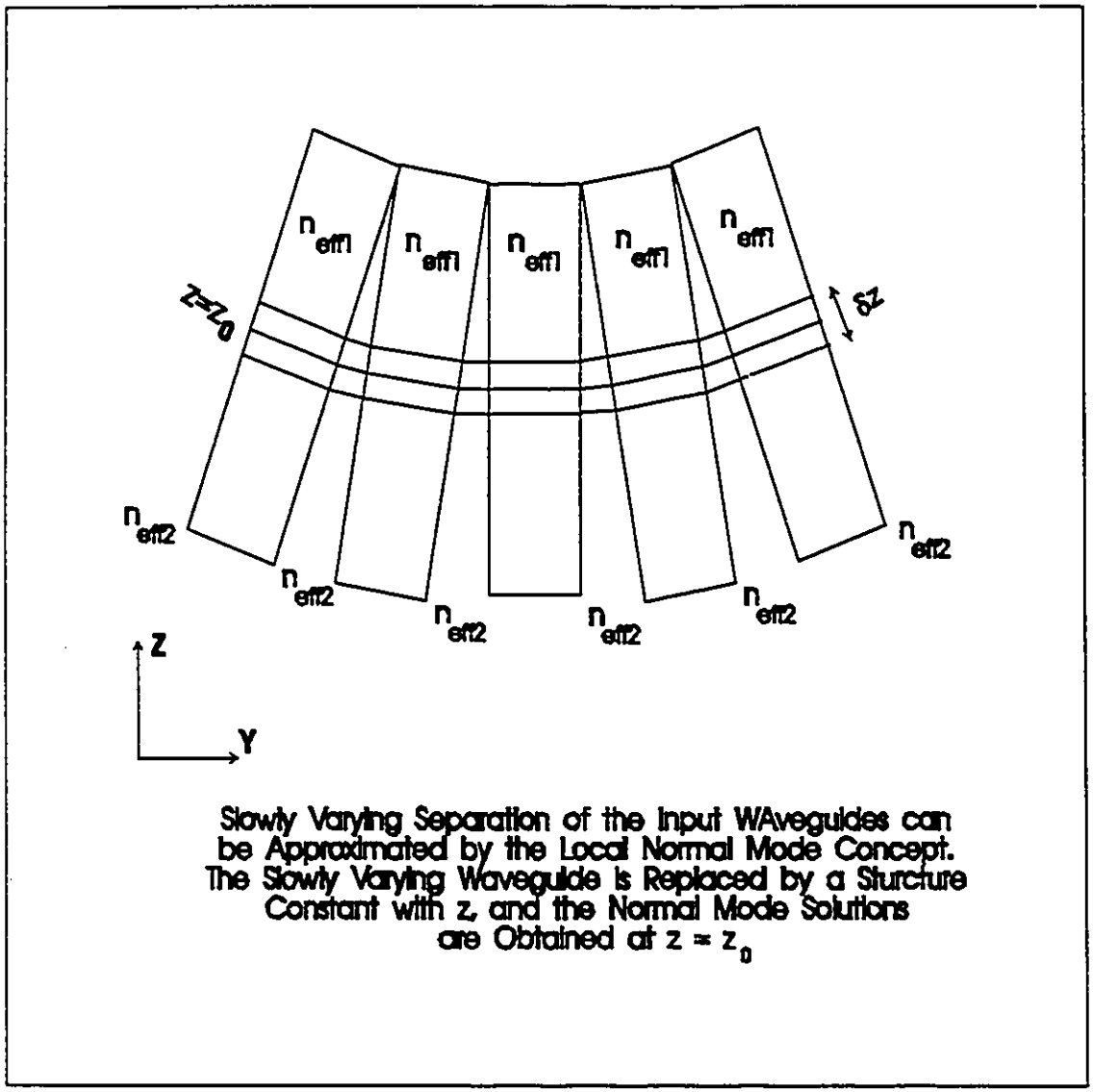

Fig.4.4: Slowly Varying Waveguide Structure

In the transition region, the separation between the input waveguides gradually decreases from 5.25 μm to zero. The mutual coupling becomes stronger as the separation decreases. As the separation decreases slowly, the propagation constants and the normal modes also

vary in the direction of propagation. At a waveguide position z_0, the normal modes of the structure are calculated as if it does not vary with z as shown in Fig.4.4. These normal modes solutions are then said to be the local normal modes of the actual varying waveguides at the position $z = z_0$ [35].

Since the transition is extremely gradual, it will cause negligible power transfer between the normal modes [35]. The power in a given local mode will stay in that mode throughout the whole transition. As a local mode propagates, its phase also increases across each section by the product of the propagation constant and the section δz. Consequently, the phase at an arbitrary position along the propagation is a sum of such products [36]. Consequently, the field distribution over N waveguides due to the i^{th} input waveguide is approximated as :

$$H^i(y,z)=\sum_{v=1}^{N}\sum_{l=1}^{N}\sum_{m=1}^{M}\alpha_{il}H_v(y,z)\exp[-\beta_{vm}\delta z] \qquad (4.13)$$

where

β_{vm} is the longitudinal propagation constant of the normal mode v at section m.

M = 120 is the total number of sections in the transition

δz = 34 μm

Table 3 summarised the longitudinal propagation constant when the spacings between the waveguides are 5.25 μm and zero μm. The normal mode A has the greatest longitudinal propagation constants (β) amongst other normal modes. When the spacing between the waveguides becomes smaller, the longitudinal propagation constant (β) are also smaller. When the waveguides are far apart, the longitudinal propagation constants between the 5 normal modes are wider spread than in narrow spacings. This can be observed in Appendix K which gives different propagation constant (β_{vm}) for 120 different regions. From equation (4.13), both amplitude and phase response prior to diffraction are given in Fig.4.5 and Fig.4.6, respectively.

	Longitudinal Propagation Constant (β)	
Normal Mode (ν)	Spacing between Waveguide (S) = 5.25μm	Spacing between Waveguide (S) → 0 μm
A (1)	6.96699677	6.9563355
B (2)	6.96371370	6.9560867
C (3)	6.95830164	6.9557280
D (4)	6.95088541	6.9553436
E (5)	6.94178602	6.9550435

Table 3: Longitudinal Propagation Constants of the Five Normal Modes at the Beginning and End of the Coupling Region

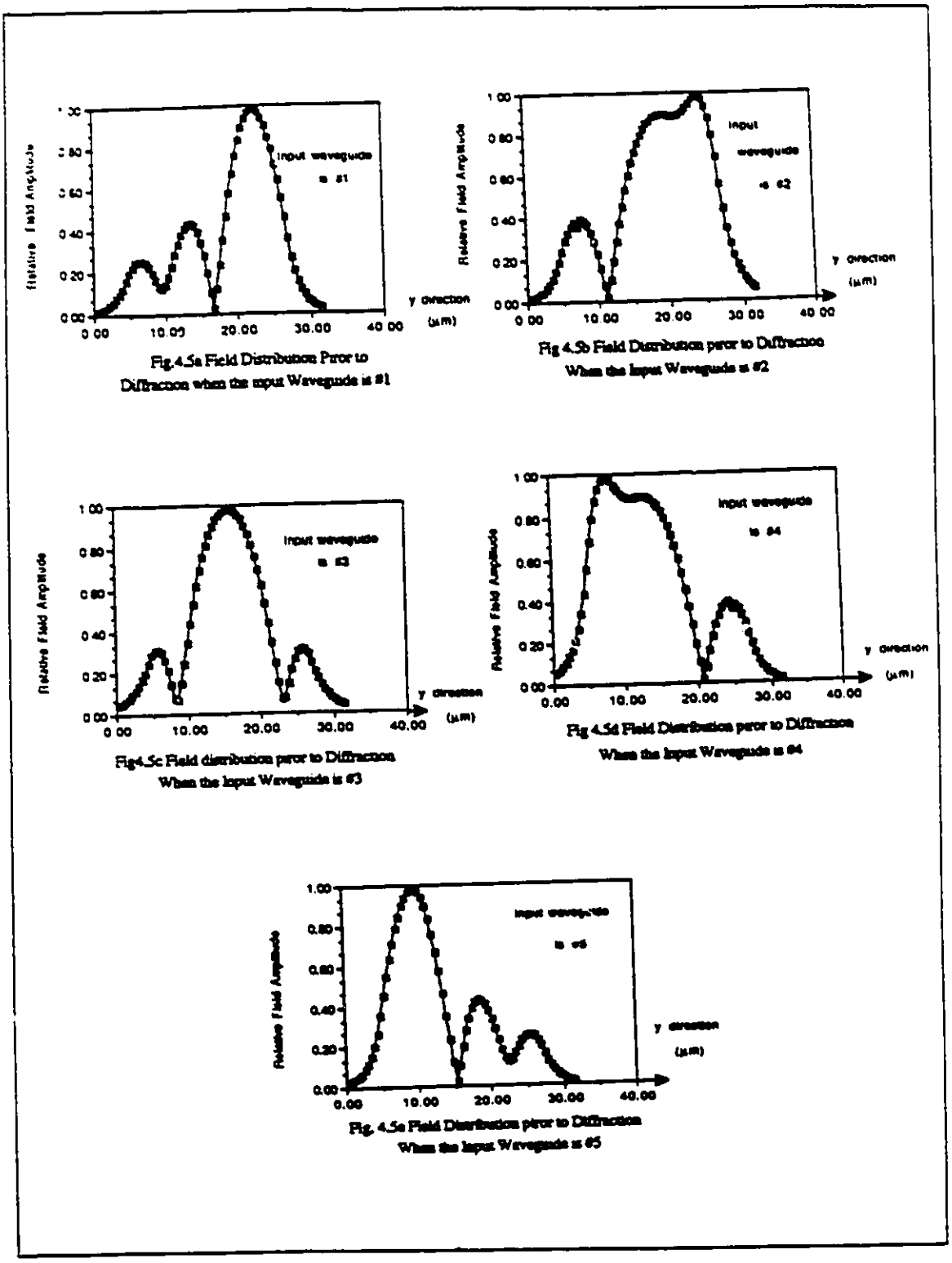

Fig.4.5a Field Distribution Prior to Diffraction when the input Waveguide is #1

Fig.4.5b Field Distribution prior to Diffraction When the Input Waveguide is #2

Fig4.5c Field distribution prior to Diffraction When the Input Waveguide is #3

Fig.4.5d Field Distribution prior to Diffraction When the Input Waveguide is #4

Fig. 4.5e Field Distribution prior to Diffraction When the Input Waveguide is #5

Fig.4.5: Field Amplitude Prior to Diffraction

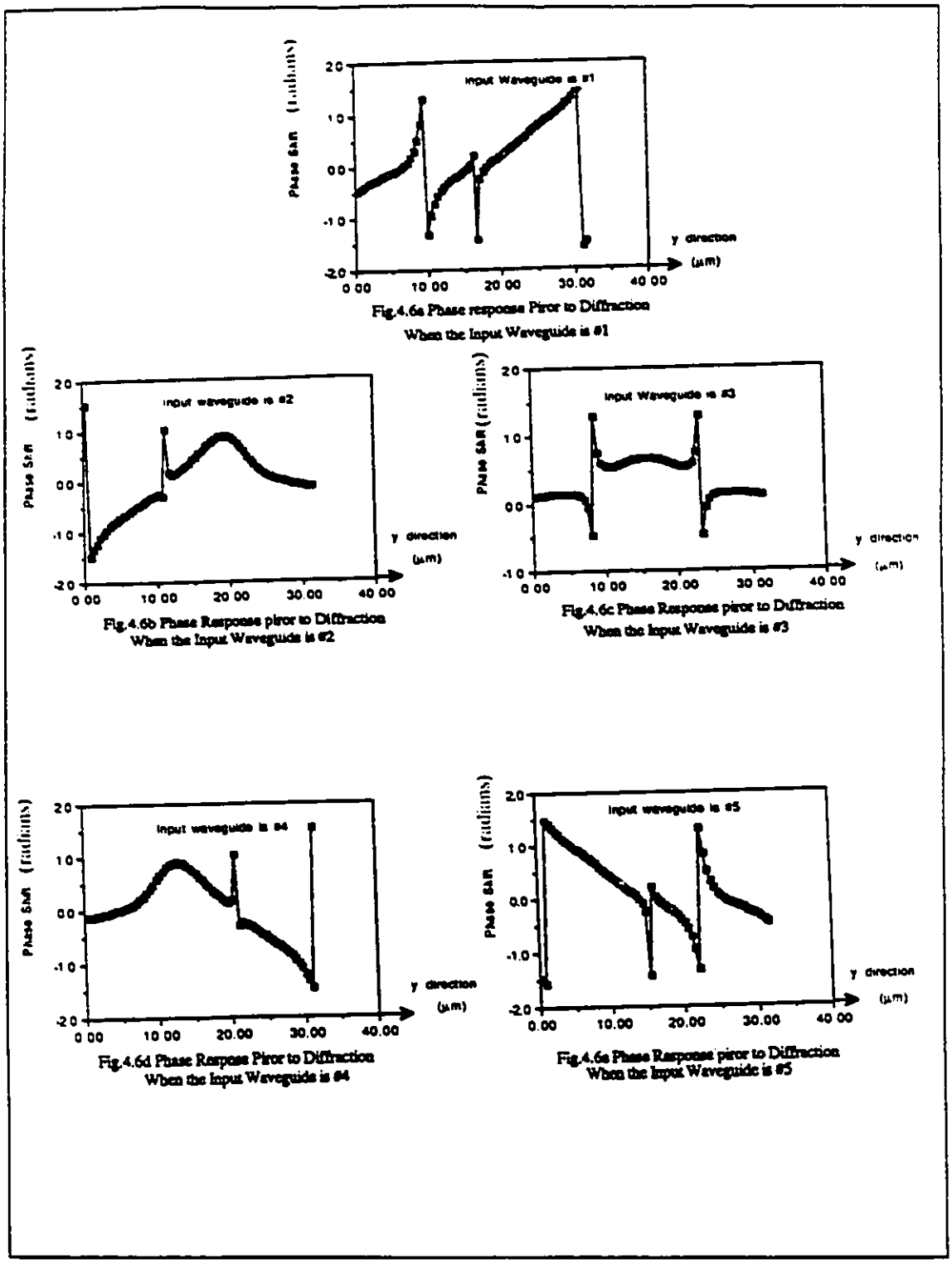

Fig.4.6a Phase response Piror to Diffraction When the Input Waveguide is #1

Fig.4.6b Phase Response piror to Diffraction When the Input Waveguide is #2

Fig.4.6c Phase Response piror to Diffraction When the Input Waveguide is #3

Fig.4.6d Phase Respose Piror to Diffraction When the Input Waveguide is #4

Fig.4.6e Phase Response piror to Diffraction When the Input Waveguide is #5

Fig.4.6: Field Phase Prior to Diffraction

4.5 Diffraction Region

In the diffraction region, the refractive index is almost constant everywhere as in an almost unbounded dielectric medium so that the fields can be expressed as individual plane waves [37]. For a planar structure, the magnetic field is given as :

$$H(y,z)=H_0\exp[-j(k_2y+\beta z)] \tag{4.14}$$

where H_0 is the wave amplitude constant

$$k_2^2+\beta^2=k_0^2 \tag{4.15}$$

From [37],

$$H(y,z) = \int_{-\infty}^{\infty} H(k_2)\exp[-j(k_2y+\beta z)]\, dk_2 \tag{4.16}$$

At z = 0

$$H(y,0)=\int_{-\infty}^{\infty} H(k_2)\exp(-jk_2y)dk_2 \tag{4.17}$$

Thus, the weighting coefficients $H(k_y)$ of the plane waves are the Fourier transform of the transverse field distribution at the beginning of the diffraction region. Thus,

$$H(k_2)=\frac{1}{2\pi}\int_{-\infty}^{\infty} H(y,0)\exp(jk_2y)dk_2 \tag{4.18}$$

The diffraction patterns on the receiving side of the coupler are illustrated in Fig.4.7. The length of the diffraction region, D is designed to reduce the spill-over, mode mismatch and the reflection loss as shown in Fig.4.7. D is designed as:

$$D=\frac{H}{2\sin\theta} \tag{4.19}$$

where

H is the width of the receiving aperture

θ is the diffraction angle

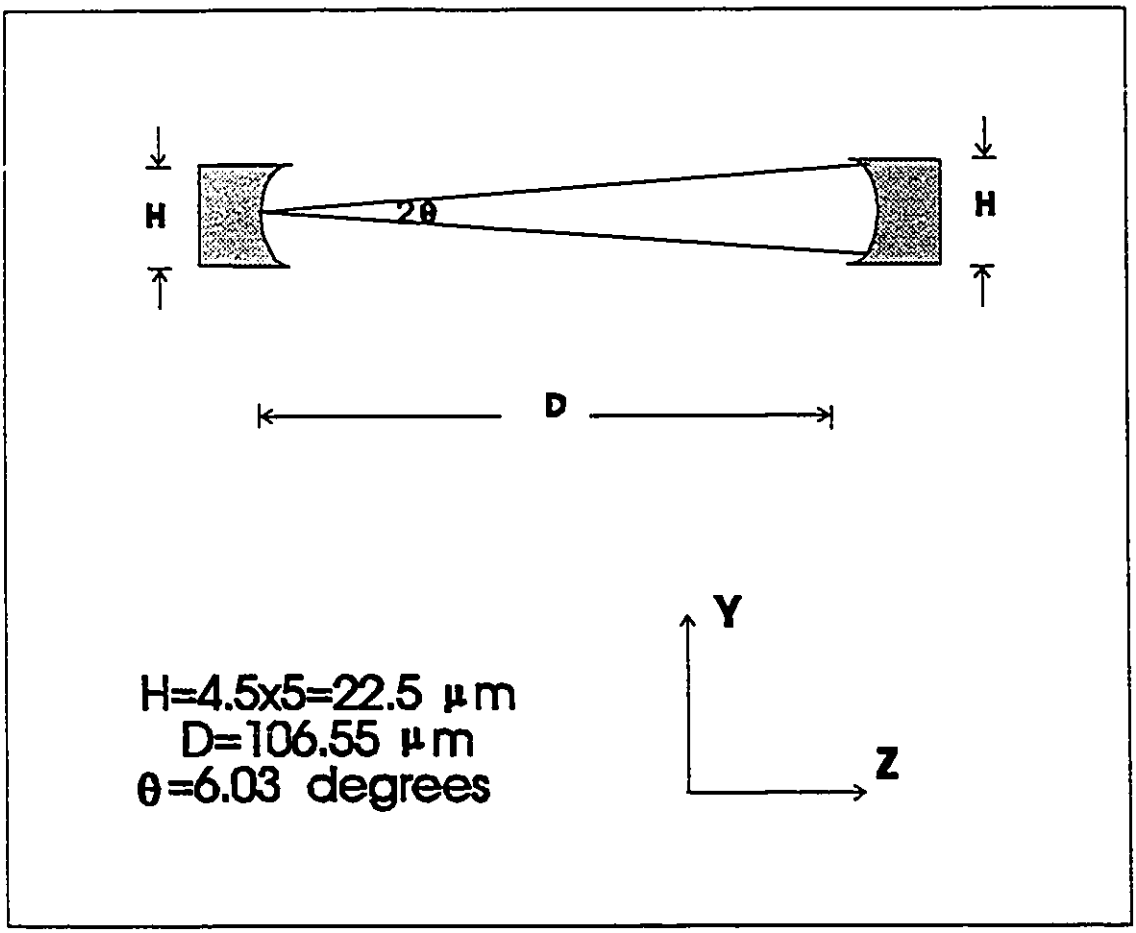

Fig.4.7: Diffraction Region of the Star coupler

Theoretically, the length of the diffraction region must be long enough to fulfil the Fraunhofer diffraction approximation. In other words, in order to use the Fourier Transform to calculate the far field pattern, D must be as follows [38]:

$$D > \frac{k(z_1^2 + y_1^2)_{max}}{2} \qquad (4.20)$$

where

z_1 and y_1 are co-ordinates in the far field

However, Fraunhofer diffraction patterns can be observed at distances much shorter than implied by the above formula, provided that the receiving aperture is illuminated by a circular wave converging towards the receiving element as shown in Fig.4.7. [35] gives the planar structure arrangements producing the Fourier Transform with the Fresnel diffraction approximation for a large N.

4.6 Power-dividing Branch Waveguide

The purpose of this region is to distribute the received power to the output ports evenly. On the receiving side, the power-dividing waveguide is assumed to be single-mode.

According to [8], for a branching waveguide with index asymmetry, the normal modes will evolve to a stage of having most of their power associated with only a single waveguide if the separation between the waveguides is large enough. However, with regards to a perfectly symmetric (both index and separation) branching waveguide as shown in Fig.4.8, the normal modes maintain a stage of evenly dividing their power between the branches at any separation.

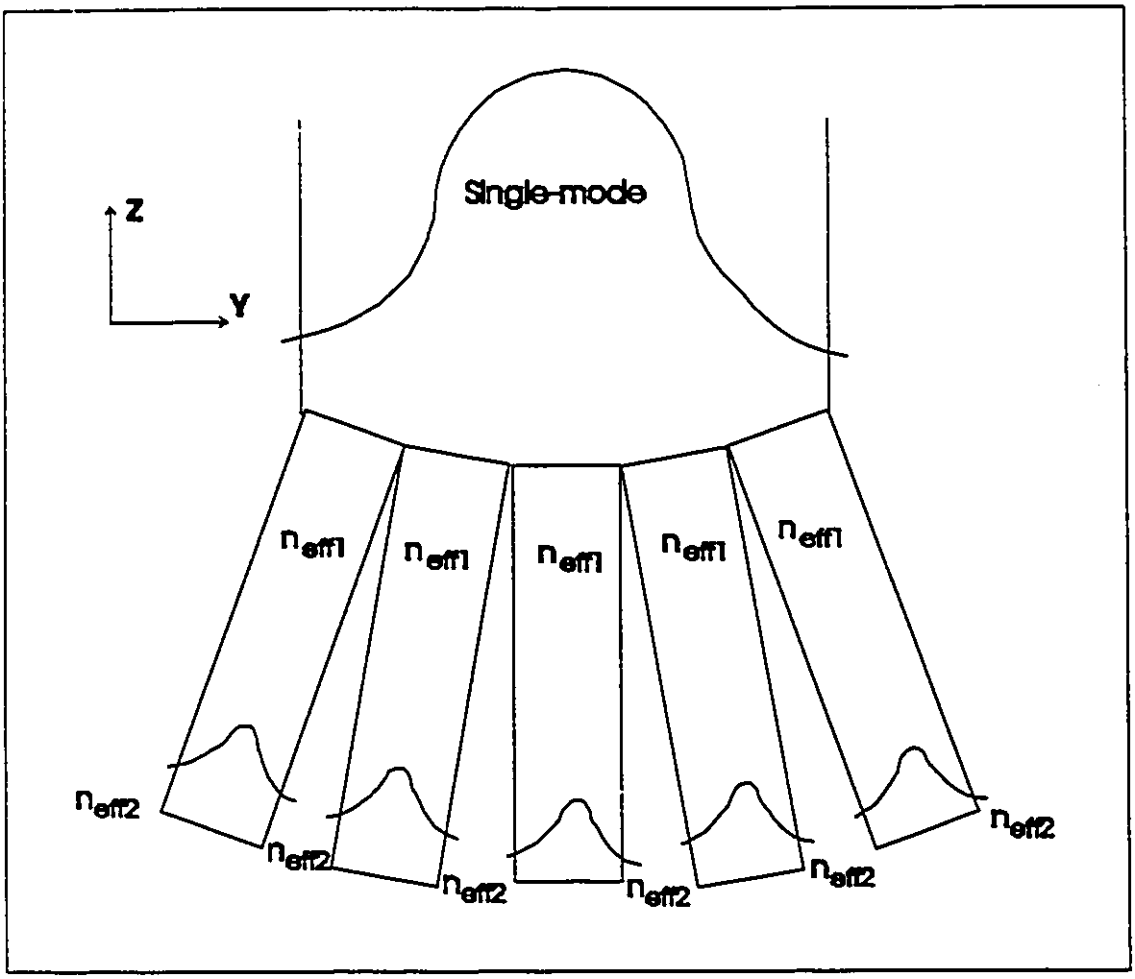

4.7 Loss Consideration

Additional to splitting loss, there are other losses related to the device.

4.7.1 Spill-Over Loss

Only a fraction of the radiated power from the transmitting waveguide is intercepted by the receiving element; the remaining is lost due to spill-over. From Fig.4.9a to Fig.4.9e, the shaded area represents the spill-over loss when the radiating angle is 6.03 degrees. The spill-over is dependent on the i^{th} waveguide with input power, length of the transition region, and length of the diffraction region. Theoretically, if the diffraction region is long

enough, the spill-over loss can be eliminated, i.e. the receiving waveguide is far enough to collect all the power from the transmitting waveguide. However, the received radiation pattern is different from the single-mode of the receiving waveguide. The difference will create mode-mismatch loss. Thus, the length of transition region and diffraction must be optimum to minimize both the spill-over and the mode-mismatch loss with input to different waveguides.

4.7.2 Mode-Mismatch Loss

The fundamental mode of the receiving waveguide can only accept a fraction of the incident power illuminating the element aperture because the transverse mode is different from those of the far field pattern as shown in Fig.4.9a to Fig.4.9e. The area under the single-mode pattern is equal to the area under the received radiation pattern. Any radiation which does not entre into the single-mode pattern region is the mode-mismatch loss. Computer simulations were performed to vary the transition and the diffraction regions to minimise the mode-mismatch loss with different input waveguides. The central shaded area represents the mode-mismatch loss which is dependent on the i^{th} input power waveguide excitation. The mode-mismatch and spill-over loss are summarised in Table 4 when the length of transition region is 4.08 mm and the length of the diffraction region is 106.55 μm.

input into the waveguide	Spill-over Loss	Mismatch Loss	Total Loss
#1	23.8 %	16.9 %	40.7 %
#2	22.2 %	21.7 %	43.9 %
#3	21.2 %	19.1 %	40.3 %
#4	22.2 %	21.7 %	43.9 %
#5	23.8 %	16.9 %	40.7 %

Table 4: Estimated Loss with Input to Different Waveguide

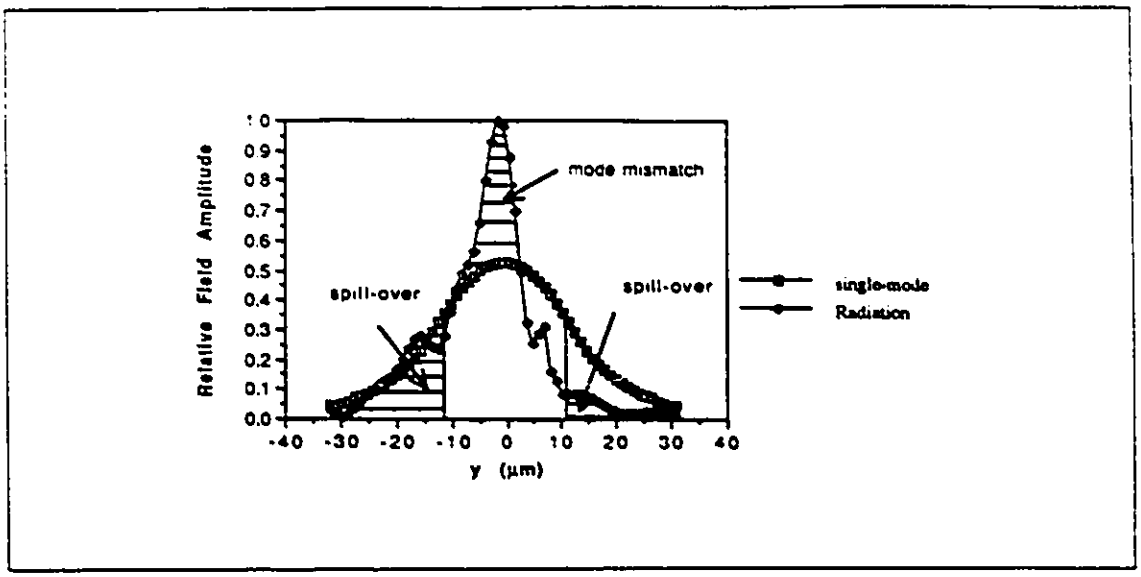

Fig.4.9a: Loss Analysis of the Star Coupler with Input to the 1st Waveguide

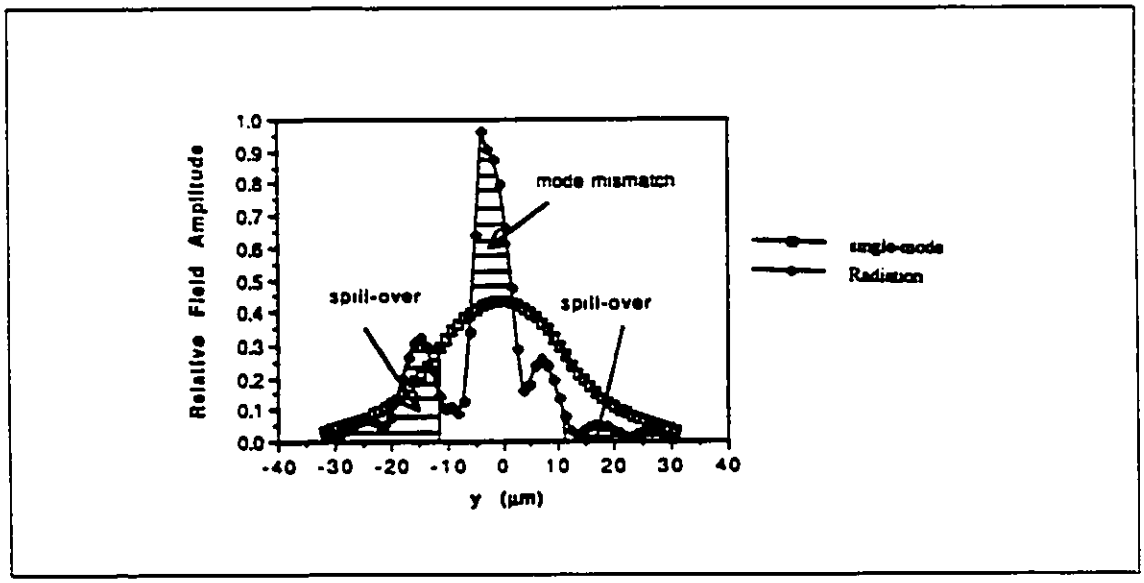

Fig.4.9b: Loss Analysis of the Star Coupler with Input to the 2nd Waveguide

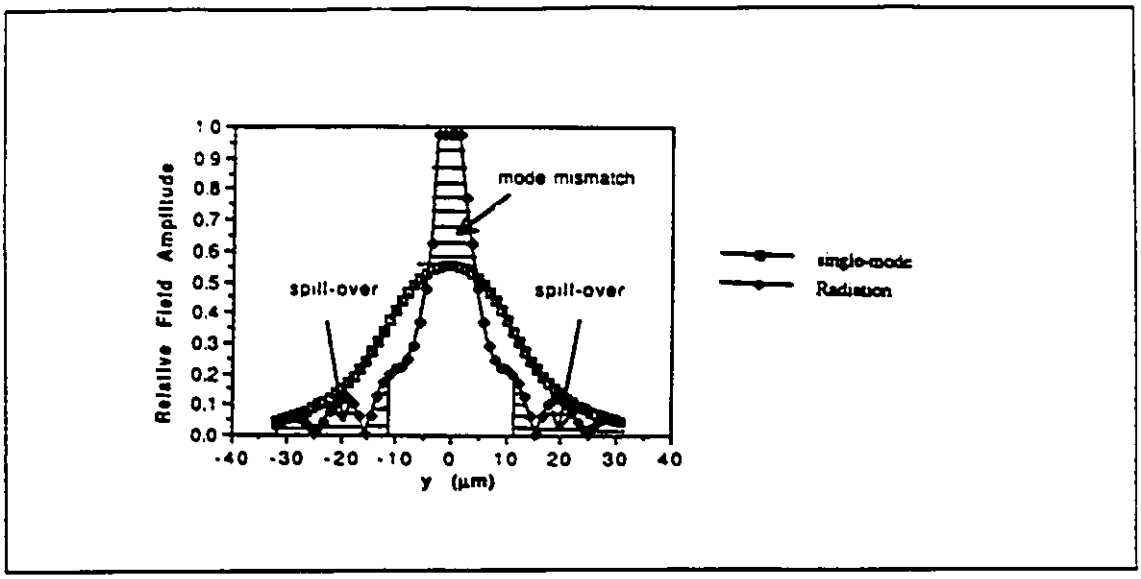

Fig.4.9c: Loss Analysis of the Star Coupler with Input to the 3rd Waveguide

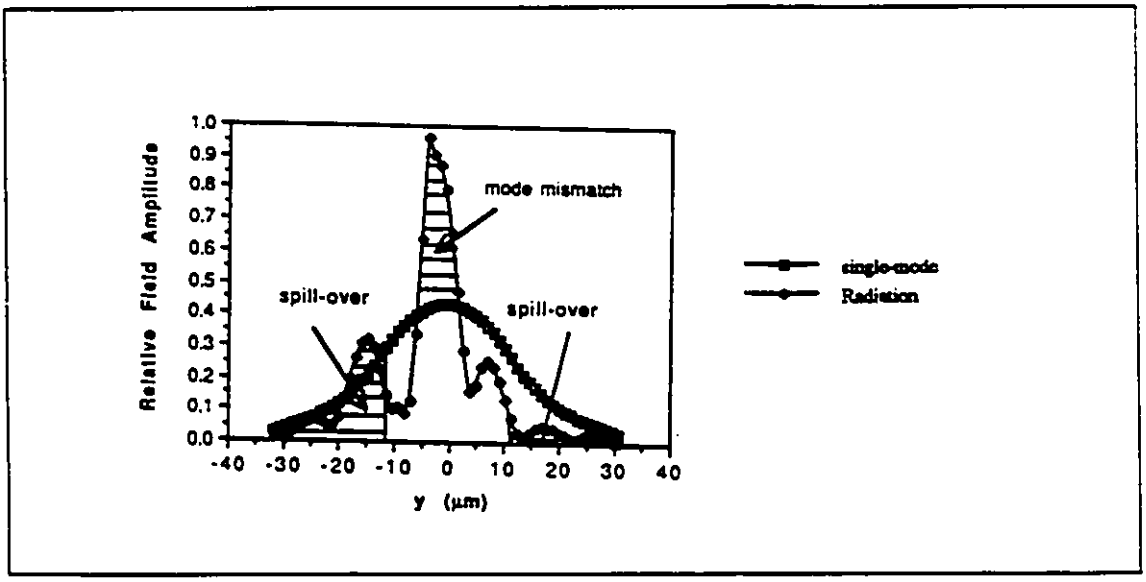

Fig.4.9d: Loss Analysis of the Star Coupler with Input to the 4th Waveguide

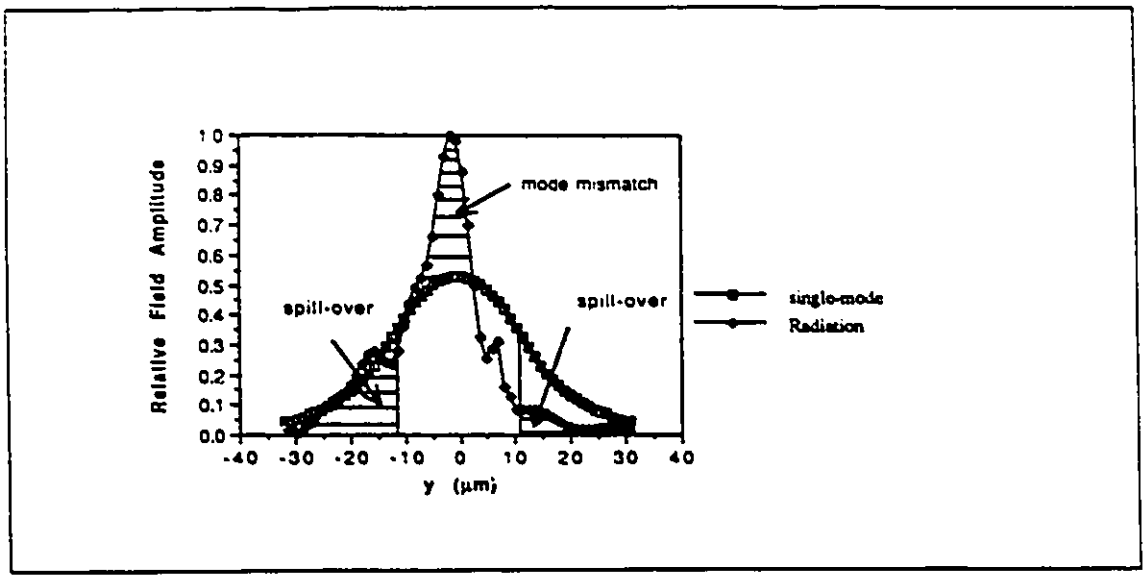

Fig.4.9e: Loss Analysis of the Star Coupler with Input to the 5th Waveguide

4.8 Conclusions:

A slab waveguide optical star coupler for single mode fibres was modelled. the local-mode fields were used to approximate the exact fields for the slow variation of the separation in the transition region. The resultant fields then diffract to the receiving waveguides. Simulation results show that when the length of the transition region is 4.08 mm, the far field pattern for different input power waveguides were obtained as shown in Fig.4.9. The length of the diffraction region is designed to eliminate the spill-over, mode-mismatch and reflection loss. When the maximum diffracted angle is 6.03 degrees, the loss is summarised in Table 4. For different transition and diffraction length, one may achieve low loss for one particular input waveguide but high loss for other input waveguides. This may crate an undesirable loss deviation amongst different waveguides. Due to the symmetry of the coupler structure, the loss with input to the 1st waveguide is exactly the same loss with the fifth input power waveguide as shown in Fig.4.9a to Fig.4.9e. The loss from the second input power waveguide is exactly the same loss from the fourth input power waveguide as shown in Fig.4.9b and 4.9d. The other important criterion for a coupler is the minimum loss deviation among the output ports. This can be accomplished by making perfect index symmetry on the branching waveguide on the receiving side.

5 Conclusions and Suggestions

5.1 Conclusions

In this thesis, we investigated the field distribution for an N-waveguide coupler in terms of the normal modes [3]. By solving Maxwell's equations in each layer and making use of the fact that the normal modes are either symmetric or anti-symmetric in a symmetric waveguide system, the field distributions of normal modes can be obtained. When the longitudinal propagation constants vary in the direction of propagation, the normal modes of the structure are replaced by the concept of a locally normal mode [4].

Moreover, for a slowly varying waveguide structure with propagation distance, negligible power transfer occurs between the normal modes [5]. Thus, power entered in the first-order local normal mode will end up in the first-order local normal mode.

Furthermore, the plane wave weighting coefficients are given by the Fourier transform of the beam transverse distribution before diffraction [7]. Only a fraction of the radiated power from the transmitting waveguide is intercepted by the receiving waveguide; the remainder is lost due to the spill-over as shown in Fig.4.9. Theoretically if the diffraction region is long enough, the spill-over loss can be eliminated. However, the received radiation pattern is different from the single-mode pattern of the receiving waveguide. The difference creates mode-mismatch loss. Thus, the length of the transition and diffraction regions must be optimised to minimize both spill-over and mode-mismatch losses. For a branching waveguide with refractive index and separation symmetry, the normal modes evenly divide their power between the branches at any separation. Thus, the received power will be distributed to the

output ports evenly [8].

Simulation results show that when the length of the transition region and of the diffraction region are 4.08 mm and 106.55 μm respectively, total loss is the minimum (spill-over is and mode-mismatch). the total losses are between 40.7% to 43.9% The received radiation patterns with input to the different waveguides are obtained as shown in Fig.4.9. The length of the diffraction region is designed to minimise the spill-over and the mode-mismatch losses. When the maximum diffracted angle is 6.03°, these loss are summarised in Table 4. The results are quite similar to those from [18]. The other important criterion for a coupler is the minimum loss deviation among the output ports. This can be accomplished by making symmetric branching waveguides (both refractive index and physical separation) on the receiving side as shown in Fig.4.8.

5.2 Suggestions for further Work

The effective Index Method, since its discovery, has been widely applied to different waveguides. The accuracy of the effective index method depends on several factors such as large aspect ratios ($w/t > 1$) [18], an operating frequency which is far from cut-off frequency [28], and a small difference between the relative refractive indices involved [27]. Despite that, it is a widely adopted approximation technique to determine propagation constants and field distributions of fundamental modes in optical waveguides It is suggested that to gain more accuracy in the results numerical methods such as finite element method [19-20] should be applied to determine the propagation constants and field distributions of the fundamental modes. Both the effective index method and the finite element method [19-20] can give both propagation constants and the field distributions. Unlike the effective index method, the only limitation is that the operating frequencies are close to the cut off frequency of the mode under consideration. Since the model in this thesis is not constrained by N=5, using a large number of input and output waveguide, (N>5) is also suggested for future research.

Appendix A

Derivation of the Glancing Incident Angle in the Core (ξ_c)

The phase condition of the fundamental (0-th order) mode is illustrated in Fig.2.1 and expressed as:

$$2k_0 n_c d_e \sin\xi_c + \chi_1 + \chi_2 = 0 \qquad \text{(A.1)}$$

where

k_0 is the wavenumber in vacuum

ξ_c is the propagation angle of the fundamental mode in the core

n_c is the refractive index in core

d_e is the equivalent thickness of core

χ_1 is the phase shift at the interface between air and core

χ_2 is the phase shift at the interface between core and cladding layers

The phase shifts are given [15] as:

$$\chi_1 = 2\tan^{-1}\left(\frac{\alpha_{ax}}{k_{cx}}\right) \qquad \text{(A.2)}$$

$$\chi_2 = 2\tan^{-1}\left(\frac{\alpha_{1x}}{k_{cx}}\right) \qquad \text{(A.3)}$$

where

α_{ax} and α_{1x} are the transverse attenuation constant in the air and the cladding layers.

k_{cx} is the transverse propagation constant in the core

If the core is thick enough, the fundamental mode has a negligible tail in the air region, i.e. both $\alpha_{ax} \approx \alpha_{1x} \approx \infty$. Thus, both χ_1 and $\chi_2 \approx \pi$. As a result, the phase

condition of the fundamental (0-th order) mode is expressed as:

$$\sin\xi_c \approx \frac{\lambda}{2n_c d_c} \tag{A.4}$$

The equation (2.2) has been derived.

Appendix B

Derivation of Equivalent Core Thickness (d_e)

According to [15] and Fig.2.3, the physical core thickness can be expressed in terms of the transverse propagation and attenuation constant as follows:

$$k_{cx}d = \tan^{-1}\left(\frac{\alpha_{ax}}{k_{cx}}\right) + \tan^{-1}\left(\frac{\alpha_{1x}}{k_{cx}}\right) \tag{B.1}$$

By definition, the transverse propagation constant, k_{cx} is given as:

$$k_{cx} = k_0 n_c \sin\xi_c \tag{B.2}$$

Combining (B.1) and (B.2),

$$d = \frac{\tan^{-1}\left(\frac{\alpha_{ax}}{k_{cx}}\right) + \tan^{-1}\left(\frac{\alpha_{1x}}{k_{cx}}\right)}{k_0 n_c \sin\xi_c} \tag{B.3}$$

Recall (A.4)

$$d_e \approx \frac{\lambda}{2n_c \sin\xi_c} \tag{B.4}$$

Combining (B.3) and (B.4), the equivalent core thickness is given as follows:

$$d_e = d + \frac{2\pi - \chi_1 - \chi_2}{2k_0 n_c \sin\xi_c} \tag{B.5}$$

where χ_1 is the phase shift at the interfaces between air and the core and is defined by (A.2)

χ_2 is the phase shift at the interfaces between the core and the second cladding and is defined by (A.3)

The penetration of the field into the cladding layers can be neglected under the extremely high reflecting condition ($\alpha_{1x} \to \infty$)

Thus, the equivalent core thickness can be approximated as follows:

$$d_e = d + \frac{1}{\alpha_{ax}} \tag{B.6}$$

According to [29], the phase shift of TE mode at the interface between the core and air is as follows:

$$\tan\chi_1 = \frac{\sqrt{n_c^2\cos^2\xi_c - n_0^2}}{n_c\sin\xi_c} \tag{B.7}$$

Combining equation (B.5) and (B.7) and assuming the glancing incident angle is very close to 90 degrees.

$$\frac{\alpha_{ax}}{k_0} = \sqrt{n_c\cos^2\xi_c - n_0^2} \approx \sqrt{n_c - n_0^2} \tag{B.8}$$

Putting equation (B.8) into (B.6), the equivalent core thickness (d_e) in Fig.2.3 is :

$$d_e = d + \frac{1}{k_0(n_c^2 - n_0^2)^{\frac{1}{2}}} \approx d + \frac{\lambda}{2\pi(n_c^2 - n_0^2)^{\frac{1}{2}}} \tag{B.9}$$

The equation (2.3) has been derived.

Appendix C

Derivation of the Optimum First Cladding Layer Thickness (t_1)

According to [16], maximum reflection will occur in Fabry-Perot interferometer under antiresonant condition.

In a Fabry-Perot interferometer, the phase delay between two partial waves is expressed as the product of wavenumber and path length as shown in Fig.2.2.

$$\zeta = 2k_0 n_1 t_1 \sin\xi_1 = 2k_{1x} t_1 \sin\xi_1 \qquad (C.1)$$

where

k_{1x} is the wavenumber in the first cladding

$2t_1\sin\xi_1$ is the path length

Considering the reflection characteristics of a Fabry-Perot etalon, the reflection is unity whenever

$$\zeta = \frac{\pi}{2} + L_1\pi \qquad (C.2)$$

where $L_1 = 0,1,2 \ldots$.

Putting equation (C.2) into (C.1),

$$t_1 = \frac{\pi(\frac{1}{2} + L_1)}{\sin\xi_1 k_{1x}} \qquad (C.3)$$

By Snell 's Law

$$\cos\xi_1 = \frac{n_c \cos\xi_c}{n_1} \qquad (C.4)$$

$$\sin\xi_1 = \sqrt{1 - \frac{n_c^2 \sin^2\xi_c}{n_1^2}} \qquad (C.5)$$

Combining equation (C.3) and (C.4), the optimum 1st cladding (t_1) is:

Combining (C.4) and (C.5)

$$t_1 \approx \frac{\pi(\frac{1}{2} + L_1)\lambda}{2\pi n_1}(1 - n_c^2 \sin^2 \xi_c)^{-\frac{1}{2}} \qquad \text{(C.6)}$$

Putting equation (C.6) into (A.4), the optimum 1st cladding can be approximated as follows:

$$t_1 \approx \frac{\lambda}{4n_1}(2L_1 + 1)[1 - (\frac{n_c^2}{n_1^2}) + \frac{\lambda^2}{4n_c^2 d_e^2}]^{-\frac{1}{2}} \qquad \text{(C.7)}$$

The equation (2.4) has been derived.

Appendix D

Derivation of the Optimum length of the Second Cladding (t_2)

Referring Fig.2.2, for antiresonant (maximum reflection) the length of second cladding can be expressed as follows:

$$t_2 = \frac{\pi(\frac{1}{2} + L_2)}{\sin\xi_2 K_{2x}} \tag{D.1}$$

where

L_2 = 0,1,2,3.....

k_{2x} is the wavenumber in the 2nd cladding layer

Recall (A.4)

$$\sin\xi_2 = \frac{\lambda}{2n_c d_c} \tag{D.2}$$

Putting (D.1) into (D.2), t_2 can be expressed as follows:

$$t_2 = \pi(\frac{1}{2} + L_2)(\frac{2n_c d_c}{\lambda})(\frac{\lambda}{2\pi n_2}) = d_c(\frac{1}{2} + L_2) \tag{D.3}$$

The equation (2.5) has been derived.

Appendix E

Derivation of the Dispersion Equation of ARROW Using transverse Resonant Method

The input admittance of an arbitrary transmission line is given by [17]

$$Y_{in}(x) = Y_0 \frac{Y_l + Y_0 \tanh(\gamma x)}{Y_0 + Y_l \tanh(\gamma x)} \tag{E.1}$$

where Y_0 is the characteristic admittance of the line

Y_l is the load admittance of the line

γ is the complex transverse propagation constant

The complex transverse propagation constant in mth layer, γ_m, is given by [17]

$$\gamma_m = \alpha_m + j\kappa_m = (k_z^2 - k_0^2 n_m^2)^{\frac{1}{2}} \tag{E.2}$$

where k_z is the complex propagation constant

k_0 is the wavenumber in vacuum

n_m is the refractive index of the m layer

Moreover, k_z is defined as follows:

$$k_z = k_0 N_{eff} = k_0 n_{eff} + j\frac{\alpha}{2} \tag{E.3}$$

where N_{eff} is the complex effective index

n_{eff} is the real part of N_{eff}

α is the propagation loss (Np/cm)

Thus, when $n_{eff} > n_m$,

$$\gamma_m = \alpha_m + j\kappa_m \tag{E.4}$$

Meanwhile for $n_{eff} < n_m$,

$$\gamma_m = j(\kappa_m - j\alpha_m) \tag{E.5}$$

As result,

$$\gamma_m = k_0(N_{eff}^2 - n_m^2)^{\frac{1}{2}} \tag{E.6}$$

Referring fig.2.7, the transmission line equivalent circuits are used to find input admittance at the boundaries of different layers.

E.1 Input Admittance at 2nd Cladding/Substrate Boundary looking downward, $Y_{in,3}$

$$Y_{in,3} = Y_3 \frac{Y_{lb} + Y_3 \tanh(\gamma_3 l)}{\gamma_3 + Y_{lb} \tanh(\gamma_3 l)} \tag{E.7}$$

where l and Y_{lb} are the thickness and equivalent load of the substrate respectively

γ_3 is given as

$$\gamma_3 = jk_0(n_3^2 - N_{eff}^2)^{\frac{1}{2}} = j\kappa_3 + \alpha_3 \tag{E.8}$$

Putting equation (E.8) into (E.7),

$$\tanh(\gamma_3 l) = \frac{\tanh(\alpha_3 l) + j\tan(\kappa_3 l)}{1 + j\tanh(\alpha_3 l)\tan(\kappa_3 l)} \tag{E.9}$$

Compared with the wavelength of light, the substrate is infinite thick. When $l \to \infty$, equation (E.7) becomes

$$Y_{in,3} \approx Y_3 \tag{E.10}$$

According to [17], characteristic admittance is expressed as

$$Y_3 \approx -j\frac{\gamma_3}{\omega\mu_0} \tag{E.11}$$

where ω is the angular frequency

μ_0 is permeability in air

E.2 Input Admittance at the Air/Core Boundary Looking Upward, $Y_{in,a}$

$$Y_{in,a} \approx Y_a \tag{E.12}$$

E.3 Input Admittance at the 1st/2nd Cladding Boundary Looking Downward, $Y_{in,2}$

$$Y_{in,2} = Y_2\frac{Y_{in,3}+Y_2\tanh(\gamma_2 t_2)}{Y_2 + Y_{in,3}\tanh(\gamma_2 t_2)} = (-j\frac{\gamma_2}{\omega\mu_0})\frac{\gamma_3 + \gamma_2\tanh(\gamma_2 t_2)}{\gamma_2 + \gamma_3\tanh(\gamma_2 t_2)} \tag{E.13}$$

When $n_{eff} >> \alpha$

$$\gamma_2 \approx k_0(n_{eff}^2 - n_2^2)^{\frac{1}{2}} = j\kappa_2 \tag{E.14}$$

Thus, equation (E.13) can be approximated as:

$$Y_{in,2} \approx (\frac{\kappa_2}{\omega\mu_0})\frac{\kappa_3 + j\kappa_2\tan(k_2 t_2)}{\kappa_2 + j\kappa_3\tan(\kappa_2 t_2)} \tag{E.15}$$

When the cladding layers are optimum, the Fabry-Perot Etalon is in antiresonant state, i.e. both $\gamma_1 t_1$ and $\gamma_2 t_2$ are equal to $\pi/2$.

Thus, equation (E.15) becomes

$$Y_{in,2} = \frac{\kappa_2^2}{\omega\mu_0\kappa_3} \tag{E.16}$$

E.4 Input Admittance at Core/1st Cladding Interface Boundary Looking Downward, $Y_{in,1}$

$$Y_{in,1} = Y_1\frac{\overline{Y_{in,2}^2} + Y_1\tanh(\gamma_1 t_1)}{Y_1 + \overline{Y_{in,2}}\tanh(\gamma_1 t_1)} \tag{E.17}$$

with

$$Y_1 = -j\frac{\alpha_1}{\omega\mu_0} \tag{E.18}$$

Thus,

$$Y_{in,1} = -j(\frac{\gamma_1}{\omega\mu_0})\frac{\overline{Y_{in,2}} + \gamma_1\tanh(\gamma_1 t_1)}{\gamma_1 + \overline{Y_{in,2}}\tanh(\gamma_1 t_1)} \tag{E.19}$$

Besides,

$$\overline{Y_{in,2}} = Y_2\frac{Y_3 + Y_2\tanh(\gamma_2 t_2)}{Y_2 + Y_3\tanh(\gamma_2 t_2)} \tag{E.20}$$

Or equation (E.20) can be written in terms of the complex transverse propagation constants as follows:

$$\overline{Y_{in,2}} = \gamma_2\frac{\gamma_3 + \gamma_2\tanh(\gamma_2 t_2)}{\gamma_2 + \gamma_3\tanh(\gamma_2 t_2)} \tag{E.21}$$

When $n_{eff} >> \alpha$,

$$\gamma_1 \approx k_0(n_{eff}^2 - n_1^2)^{\frac{1}{2}} \tag{E.22}$$

Or Y_{in1} can be written as:

$$Y_{in,1} = \frac{\kappa_1}{\omega\mu_0}\frac{\overline{Y_{in,2}} + jY_1\tan(k_1t_1)}{Y_1 + j\overline{Y_{in,2}}\tan(\kappa_1t_1)} \tag{E.23}$$

When $\kappa_1 t_1 \rightarrow \pi/2$ (antiresonant state),

$$Y_{in,1} \approx \frac{\kappa_1^2\kappa_3}{\omega\mu_0\kappa_2^2} \tag{E.24}$$

Furthermore, $\gamma_1 \gg \gamma_2$ and $\gamma_3 \gg \gamma_2$ because the refractive indexes of the 1st cladding and substrate (3.5 for Si) are much higher than that of 2nd layer (1.45 for SiO_2). As result,

$$Y_{in,1} \approx \infty \text{ for Antiresonance} \tag{E.25}$$

E.5 Input Admittance at core/1st Cladding Boundary Looking Upward, $Y_{in,c}$

Similarly, Y_{inc} can be expressed as follows:

$$Y_{in,c} = Y_c\frac{Y_{in,a} + Y_c\tanh(\gamma_c d)}{Y_c + Y_{in,a}\tan(\gamma_c d)} \tag{E.26}$$

where

$$\gamma = jk_0(n_c^2 - N_{eff}^2)^{\frac{1}{2}} = j(\kappa_c - j\alpha_c) \tag{E.27}$$

When $n_{eff} >> \alpha$,

$$\gamma_c = k_0(n_{eff}^2 - n_c^2)^{\frac{1}{2}} = j\kappa_c \tag{E.28}$$

Thus, $Y_{in,c}$ can be expressed as follows:

$$Y_{in,c} = j(\frac{\gamma_c}{\omega\mu_0})\frac{\gamma_0 + \gamma_c\tanh(\gamma_c d)}{\gamma_c + \gamma_0\tanh(\gamma_c d)} \tag{E.29}$$

Considering the interface between the core and 1st cladding, the total admittance seen from this boundary is zero. Thus,

$$Y_{in,c} = Y_{in,1} \tag{E.30}$$

Combining equation (E.29) and (E.19), we have the dispersion equation for TE modes in ARROW waveguide as follows:

$$\gamma_c\frac{\gamma_a + \gamma_c\tanh(\gamma_c d)}{\gamma_c + \gamma_0\tanh(\gamma_c d)} = \gamma_1\frac{\overline{Y_{in,2}} + \gamma_1\tanh(\gamma_1 t_1)}{\gamma_1 + \overline{Y_{in,2}}\tanh(\gamma_1 t_1)} \tag{E.31}$$

where

$$\overline{Y_{in,2}} = \gamma_2\frac{\gamma_3 + \gamma 2\tanh(\gamma_2 t_2)}{\gamma_2 + \gamma_3\tanh(\gamma_2 t_2)} \tag{E.32}$$

The Equation (2.25) has been derived.

When both cladding layers are optimum for antiresonance, $Y_{in,1} \to \infty$ (as shown before). Then, the dispersion equation can be simplified as:

$$\gamma_a + \gamma_c\tan(\gamma_c d) = 0 \tag{E.33}$$

where

$$\gamma_a = \alpha_a + j\kappa_a \tag{E.34}$$

$$\gamma_c = j(\kappa_c - j\alpha_a) \tag{E.35}$$

Thus, the dispersion equation can be simplified as:

$$\kappa_c + \alpha_a \tan(\kappa_c d) \approx 0 \tag{E.36}$$

The equation (2.27) has been derived.

Appendix F

Derivation of Loss Constant, α_0 of Fundamental Mode in ARROW

Power loss per unit length of Fig.2.2 is given as follows:

$$\Delta p = S(1 - R)\sin\xi_c \qquad \text{(F.1)}$$

where S is signal power

R is the power reflectivity of cladding layer

Power carried by the plane wave inside the core is:

$$P = Sd_e\cos\xi_c \qquad \text{(F.2)}$$

According to [4], power loss coefficient ($2\alpha_0$) is

$$2\alpha_0 = \frac{\Delta P}{P} = \frac{(1 - R)\tan\xi_c}{d_e} \quad \text{Np/m} \qquad \text{(F.3)}$$

Thus, loss coefficient (α_0) is

$$\alpha_0 = \frac{2.17(1 - R)\tan\xi_c}{d_e} \quad \text{dB/m} \qquad \text{(F.4)}$$

The equation (2.28) has been derived.

Appendix G

Derivation of Loss Constant of Fundamental Mode, α_0 under Optimum Conditions

Referring Fig.2.2, the transmission medium from the core (n_c) to the 1st cladding layer (n_1), the transmission coefficient can be expressed [4] as follows:

$$\tau_{cl} = \frac{2n_1 \sin\xi_1}{n_c \sin\xi_c + n_1 \sin\xi_1} \qquad \text{(G.1)}$$

For large waveguide ($d_c >> \lambda / 2\pi$), $\sin \xi_1 \approx 0$

Putting this approximation into equation (G.1),

$$\tau_{cl} = 2\frac{n_1}{n_1} = 2 \qquad \text{(G.2)}$$

Power Transmission coefficient [4] is given as follows:

$$T_{cl} = \frac{n_c}{n_1}\tau_{cl}^2 \frac{\sin\xi_c}{\sin\xi_1} = 4\frac{n_c}{n_1}\frac{\sin\xi_c}{\sin\xi_1} \qquad \text{(G.3)}$$

By definition, Reflectivity = 1 - Power transmission coefficient. Thus,

$$R_{cl} = 1 - 4\frac{n_c \sin\xi_c}{n_1 \sin\xi_1} \qquad \text{(G.4)}$$

where R_{c1} is the reflectivity from core to 1st cladding

Similarly,

$$R_{21} = 1 - 4\frac{n_2 \sin\xi_2}{n_1 \sin\xi_1} \qquad \text{(G.5)}$$

where R_{21} is the reflectivity from 2nd cladding to 1st cladding

Similarly,

$$R_{2s} = 1 - 4\frac{n_2 \sin\xi_2}{n_s \sin\xi_s} \qquad (G.6)$$

where R_{2s} is the reflectivity from 2nd cladding to substrate

With the help of equation (F.4), Loss coefficient in optimised ARROW of TE_0 mode can be expressed as:

$$\alpha_0 = 2.17(1 - R_{c1})(1 - R_{21})(1 - R_{2s})\frac{\tan\xi_c}{d_e} \qquad (G.7)$$

Combining equation (G.4), (G.5), (G.6) and (G.7),

$$\alpha_0 = 2.17(4\frac{n_c \sin\xi_c}{n_1 \sin\xi_1})(4\frac{n_c \sin\xi_c}{n_1 \sin\xi_1})(4\frac{n_c \sin\xi_c}{n_s \sin\xi_s})\frac{\sin\xi_c}{\cos\xi_c d_e} \qquad (G.8)$$

Recall (A.4)

$$\sin\xi_c = \frac{\lambda}{2n_c d_e} \qquad (G.9)$$

Since $n_2 = n_c$,

$$\sin\xi_2 - \sin\xi_c = \frac{\lambda}{2n_c d_e} \qquad (G.10)$$

By Snell's Law,

$$\sin\xi_1 = \sqrt{1 - \frac{n_c}{n_1}\sin^2\xi_c} = [1 - (\frac{n_c}{n_1})^2 [1 - (\frac{\lambda}{2n_c d_e})^2]]^{\frac{1}{2}} \qquad (G.11)$$

Similarly,

$$\sin\xi_s = [1 - (\frac{n_c}{n_s})^2 [1 - (\frac{\lambda}{2n_c d_e})^2]]^{\frac{1}{2}} \qquad (G.12)$$

Putting equation (G.9), (G.10), (G.11) and (G.12) into (G.8),

$$\alpha_0 = \frac{86859\lambda^4}{n_c d_e^5 [1 - (\frac{\lambda}{2} n_c d_e)^2]^{\frac{1}{2}}} [(n_1^2 - n_c^2) + (\frac{\lambda}{2} d_e)^2]^{-1} [(n_s^2 - n_c^2) + (\frac{\lambda}{2} d_e)^2]^{-\frac{1}{2}}$$

dB/m

(G.13)

where

λ and d_e are in μm

The equation (2.29) has been derived.

Appendix H

Derivation of the Guiding Conditions of the Normal Modes of 5-waveguide Coupler

Referring to Fig.4.2, matching the tangent components E_z and H_x

(1) y=0

Etan:

$$A_1\exp(0) = A_2 + B_2\sin(0) \tag{H.1}$$

Thus,

$$A_1 = A_2 \tag{H.2}$$

Htan:

$$-n_2k_2\sin(0) + B_2k_2\cos(0) = k_1A_1\exp(0) \tag{H.3}$$

Thus,

$$B_2 = \left(\frac{k_1}{k_2}\right) A_1 \tag{H.4}$$

(2) y=w

Etan:

$$A_2\cos(k_2w) + B_2\sin(k_2w) = A_3\cosh[k_3(w - w)] + B_3\sinh[k_3(w - w)] \tag{H.5}$$

Thus

$$A_3 = A_2\cos(k_2w) + B_2\sin(k_2w) \tag{H.6}$$

Htan:

$$-A_2k_2\sin(k_2w) + k_2B_2\cos(k_2w) = k_3A_3\sinh(k_3(w - w)) - k_3B_3\cosh(k_3(w - w)) \quad \text{(H.7)}$$

Thus,

$$B_3 = \left(\frac{k_3}{k_3}\right)[-A_2\sin(k_2w) + B_2\cos(k_2w)] \quad \text{(H.8)}$$

Similarly, all the coefficients A_1, $A_2 \cdots A_{2n+1}$, B_2, $B_3 \cdots B_{2n+1}$ can be obtained in the same way.

$$A_{2i+1} = A_{2i}\cos(k_{2i}w) + B_{2i}\sin(k_{2i}w) \quad \text{(H.9)}$$

$$B_{2i+1} = \left(\frac{k_{2i}}{k_{2i+1}}\right)[-A_{2i}\sin(k_{2i}w) + B_{2i}\cos(k_{2i}w)] \quad \text{(H.10)}$$

$$A_{2i+2} = A_{2i+1}\cosh(k_{2i+1}s) + B_{2i+1}\sinh(k_{2i+1}s) \quad \text{(H.11)}$$

$$B_{2i+2} = \left(\frac{k_{2i+1}}{k_{2i+2}}\right)[A_{2i+1}\sinh(k_{2i+1}s) + B_{2i+1}\cosh(k_{2i+1}s)] \quad \text{(H.12)}$$

$$A_{2n} = A_{2n-1}\cosh(k_{2n-1}s) + B_{2n-1}\sinh(k_{2n-1}s) \quad \text{(H.13)}$$

$$B_{2n} = \left(\frac{k_{2n-1}}{k_{2n}}\right)[A_{2n-1}\sinh(k_{2n-1}s) + B_{2n-1}\cosh(k_{2n-1}s)] \quad \text{(H.14)}$$

$$A_{2n+1} = A_{2n}\cos(k_{2n}w) + B_{2n}\sin(k_{2n}w) \quad \text{(H.15)}$$

with

$$k_{2n}^2 = n_2^2 k_0^2 - \beta^2 \tag{H.16}$$

$$k_{2i+1}^2 = \beta^2 - n_1 k_0^2 \tag{H.17}$$

where i = 1,2,....n

(3) y = nw+(n-1)s

Match the H_{tan} when y=nw+(n-1)s

$$-k_{2n}A_{2n}\sin(k_{2n}w) + k_{2n}B_{2n}\cos(k_{2n}w) = -A_{2n+1}k_{2n+1} \tag{H.18}$$

Due to the symmetry of the array structure,

$$k_{2n} = k_2 \quad ; \quad k_{2n+1} = k_1 \tag{H.19}$$

Using equation (H.19), equation becomes as follow:

$$k_2A_{2n}\sin(k_2w) + k_2B_{2n}\cos(k_2w) = -A_{2n+1}k_1 \tag{H.20}$$

Combining (H.15) and (H.20), the guidance conditions for the TM_0 mode is , therefore, given by

$$k_2W = \tan^{-1}\left(\frac{k_2B_{2n}+k_1A_{2n}}{k_2A_{2n}-k_1b_{2n}}\right) \tag{H.21}$$

When n=5, equation (H.21) is as follow:

$$\tan(k_2w) = \left(\frac{k_2B_{10} + k_1A_{10}}{k_2A_{10} - k_1B_{10}}\right) \tag{H.22}$$

Appendix I

Relative Peak Field Across the 7-waveguide Coupler

Normal Mode	Relative Peak Magnetic Field Amplitude amongst the 7-Waveguide Array						
	1st	2nd	3rd	4th	5th	6th	7th
A	1.00	1.86	2.43	2.63	2.43	1.86	1.00
B	1.00	1.41	1.00	0.00	-1.00	1.41	-1.00
C	2.43	1.81	-1.00	-2.63	-1.00	1.86	2.43
D	1.00	0.00	-1.00	0.00	1.00	0.00	-1.00
E	2.43	-1.86	-1.00	2.63	-1.00	-1.86	2.43
F	1.00	-1.41	1.00	0.00	-1.00	1.41	-1.00
G	1.00	-1.86	2.43	-2.63	2.43	-1.86	1.00

Table 5: Relative Peak Field Across the 7-Waveguide Array

Appendix J

Weighting Coefficients on Different Normal Modes with Input to Different Waveguides of a 7-waveguide Coupler Structure

Input Power	Weighting coefficients on different normal modes (A to F)						
	A	B	C	D	E	F	G
1st	1.00	3.45	2.43	3.45	2.43	3.45	1.00
2nd	1.00	2.78	1.00	0.00	-1.00	-2.78	-1.00
3rd	2.43	5.40	-2.43	-5.40	2.43	5.40	2.43
4th	1.00	0.00	1.00	0.00	-1.00	0.00	-1.00
5th	-2.43	5.40	2.43	-5.40	-2.43	5.40	-2.43
6th	1.00	-2.78	1.00	0.00	-1.00	2.78	-1.00
7th	1.00	3.45	-2.43	3.45	-2.43	3.45	1.00

Table 6: Weighting Coefficients on Different Normal Modes with Different Input Power Waveguide of a 7-waveguide Coupler Structure

Note that the summation of the weighting coefficients is always zero with input to the even numbered waveguides.

Appendix K

Longitudinal Propagation Constant of Normal Modes at Different Inter-Waveguide Separation

S (μm)	longitudinal Propagation Constant (β) under Different Normal Modes				
	Mode A	Mode B	Mode C	Mode D	Mode E
5.250000	6.9563355	6.9560867	6.9557278	6.9553436	6.9550435
5.228125	6.9563429	6.9560912	6.9557280	6.9553390	6.9550349
5.184375	6.9563579	6.9561004	6.9557284	6.9553294	6.9550172
5.140625	6.9563733	6.9561098	6.9557288	6.9553196	6.9549990
5.096875	6.9563890	6.9561194	6.9557292	6.9553096	6.9549804
5.053125	6.9564051	6.9561293	6.9557297	6.9552994	6.9549612
5.009375	6.9564216	6.9561394	6.9557315	6.9552886	6.9549416
4.965625	6.9568385	6.9561497	6.9557307	6.9552780	6.9549215
4.921875	6.9564557	6.9561604	6.9557311	6.9552670	6.9549008
4.878125	6.9564734	6.9561712	6.9557317	6.9552557	6.9548795
4.834375	6.956491	6.9561824	6.9557323	6.9552442	6.9548577
4.790625	6.9565100	6.9561938	6.9557329	6.9552322	6.9548353
4.746875	6.9565291	6.9562055	6.9557335	6.9552201	6.9548123

4.703125	6.9565484	6.9562175	6.9557342	6.9552077	6.9547887
4.659375	6.9565683	6.9562298	6.9557349	6.9551949	6.9547644
4.615625	6.9565886	6.9562424	6.9557356	6.9551819	6.9547396
4.571875	6.9566095	6.9562554	6.9557364	6.9551684	6.9547140
4.528125	6.9566095	6.9562554	6.9557364	6.9551684	6.9546878
4.484375	6.9566526	6.9562686	6.9557372	6.9551546	6.9546878
4.440625	6.956674	6.9562961	6.9557390	6.9551262	6.9546332
4.396875	6.9566978	6.9563104	6.9557399	6.9551113	6.9546048
4.353125	6.9567212	6.9563249	6.9557409	6.9550963	6.9545757
4.309375	6.9567452	6.9563399	6.9557420	6.9550907	6.9545457
4.265625	6.9567697	6.9563553	6.9557432	6.9550645	6.9545150
4.221875	6.9567948	6.9563711	6.9557443	6.9550486	6.9544834
4.178125	6.9568205	6.9563825	6.9557455	6.9550319	6.9544509
4.134375	6.9569468	6.9564037	6.9557467	6.9550148	6.9544177
4.090625	6.9568737	6.9564206	6.9557481	6.9549974	6.9543835
4.046875	6.9569012	6.9564380	6.9557495	6.9549795	6.9543483
4.003125	6.9569294	6.9556455	6.9557509	6.9549611	6.9543122
3.959375	6.9569583	6.9564742	6.9557525	6.9549423	6.9542752
3.915625	6.9569873	6.9564932	6.9557542	6.9549231	6.9542371

3.871875	6.957018	6.9565123	6.9557558	6.9549034	6.9541980
3.828125	6.957049	6.9565316	6.9557576	6.9548832	6.954157
3.784375	6.9570807	6.9565518	6.9557595	6.954862	6.954117
3.740625	6.957113	6.956573	6.9557614	6.954841	6.954407
3.696875	6.957146	6.956594	6.9557637	6.954819	6.9540307
3.653125	6.9571803	6.9566154	6.9557662	6.954798	6.9539861
3.609375	6.9572151	6.9566377	6.9557679	6.9547750	6.9539402
3.565275	6.9572510	6.9566606	6.9557703	6.9547518	6.9538929
3.521875	6.9572872	6.9566840	6.9557728	6.9547280	6.9538445
3.478125	6.9573245	6.9567080	6.9557755	6.9547037	6.9537950
3.434375	6.9573627	6.9567327	6.9557782	6.9546788	6.9537436
3.390625	6.9574018	6.9567579	6.9557812	6.9546533	6.9536911
3.346875	6.957442	6.9567838	6.9557843	6.9546273	6.9536371
3.303125	6.9574828	6.9568104	6.9557874	6.9546273	6.9536371
3.259375	6.9575245	6.9568376	6.9557908	6.9545734	6.9535247
3.215625	6.9575677	6.9568656	6.9557944	6.9545455	6.9534662
3.171875	6.9576117	6.9568942	6.9557980	6.954517(	6.9534061
3.128125	6.9576567	6.9569236	6.9558019	6.9544878	6.9533443
3.084375	6.9577028	6.9569538	6.9558060	6.9544580	6.9532157

3.040625	6.9577500	6.9569847	6.9558103	6.9544275	6.9532157
2.996875	6.9577983	6.9570164	6.9558148	6.9543963	6.9531487
2.953125	6.9578478	6.9570490	6.9558195	6.9543645	6.9530799
2.909375	6.9578985	6.9570924	6.9558245	6.9543319	6.9530093
2.865625	6.9579504	6.5711665	6.9558297	6.9542986	6.9529366
2.821875	6.9580035	6.9571519	6.9542647	6.9528621	6.9528521
2.778125	6.9580579	6.9571879	6.9558409	6.9542299	6.9527854
2.734375	6.9581136	6.9572249	6.9558470	6.9541945	6.9527070
2.690625	6.9581707	6.9572629	6.9558533	6.9541583	6.9526258
2.646875	6.9582291	6.9573019	6.9558599	6.9541213	6.9525427
2.603125	6.9582889	6.9573419	6.9558669	6.9540836	6.9524574
2.559375	9.9583503	6.9573829	6.9558742	6.9540450	6.9523698
2.515625	6.9584131	6.9574251	6.9558818	6.9540057	6.9522797
2.471875	6.9574684	6.9574683	6.9558899	6.9539656	6.9521872
2.428125	6.9585432	6.9557513	6.9558984	6.9539247	6.9520922
2.384375	6.9586108	6.957558+	6.9559072	6.9538830	6.9519947
2.340625	6.9586799	6.9576052	6.9559166	6.9538404	6.9518946
2.296875	6.9587508	6.9576533	6.9577926	6.9537971	6.9517917
2.253125	6.9588234	6.9577026	6.9537529	6.9516861	6.9597508

2.209375	6.9588978	6.9577533	6.9559473	6.9537079	6.9515777
2.165625	6.9589741	6.9578055	6.9559586	6.9536621	6.9514664
2.121875	6.9590522	6.9578589	6.9559704	6.9536155	6.9514664
2.078125	6.9591323	6.9579138	6.9559828	6.9535679	6.9512348
2.034375	6.9592144	6.9579703	6.9559958	6.9535196	6.9511144
1.990625	9.5929864	6.9580283	6.9560095	6.9534705	6.9509909
1.946875	6.9593849	6.9580879	6.9560238	6.9534205	6.9509642
1.903125	6.9594733	6.9581491	6.9560388	6.9533697	6.9507341
1.859375	6.9595640	6.9582121	6.9560547	6.9533181	6.9506008
1.815625	6.9596571	6.9582768	6.9560712	6.9532656	6.9504640
1.771875	6.9597523	6.9593432	6.9560996	6.9532125	6.9503237
1.728125	6.9598502	6.9584115	6.9561068	6.9531585	6.9501799
1.684375	6.9599507	6.9594819	6.9561259	6.9531037	6.9500325
1.640625	6.9600536	6.9585543	6.9561459	6.9530482	6.9498815
1.596875	6.9601593	6.9586286	6.9561669	6.9529919	6.9497267
1.553125	6.9602677	6.9587055	6.9561889	6.9529349	6.9495682
1.509375	6.9603789	6.9587837	6.9562121	6.9528773	6.9494059
1.465625	6.9604931	6.9588647	6.9562363	6.9528189	6.9492396
1.421875	6.9606104	6.9589479	6.9562618	6.9527600	6.9490697

1.378125	6.9607307	6.9590337	6.9562884	6.9527004	6.9488957
1.336125	6.9609493	6.9591184	6.9563153	6.9526427	6.9487250
1.290625	6.9609812	6.9592128	6.9563457	6.9525796	6.9485359
1.248625	6.9611063	6.9593026	6.9563753	6.9525209	6.9483576
1.203125	6.9612455	6.9594027	6.9564088	6.9524568	6.9483576
1.161125	6.9613775	6.9594979	6.9564413	6.9523973	6.9479744
1.115625	6.9615245	6.9596042	6.9564782	6.9523332	6.9477688
1.071875	6.9616699	6.9597095	6.9565154	6.9522597	6.9475672
1.028125	6.9618193	6.9598181	6.9565545	6.9522068	6.9473617
0.984375	6.9619730	6.9599301	6.9565955	6.9521437	6.9471523
0.940625	6.9621311	6.9600454	6.9566384	6.9520806	6.9469392
0.896875	6.9622937	6.9601645	6.9566835	6.9520173	6.9467224
0.853125	6.9624610	6.9602873	6.9567308	6.9519542	6.9465021
0.809375	6.9626331	6.9604140	6.5967804	6.9518911	6.9462783
0.765625	6.9628104	6.9605448	6.9568324	6.9618283	6.9460511
0.721875	6.9629929	6.9606798	6.9568870	6.9517658	6.9458210
0.678125	6.9631810	6.9608192	6.9569442	6.9517037	6.9455875
0.634375	6.9633746	6.9609631	6.9570043	6.9516420	6.9453514
0.590625	6.9635741	6.9637574	6.9570667	6.9515810	6.9451127

0.546875	6.9637800	6.9612656	6.9571335	6.9515208	6.9448717
0.503125	6.9639921	6.9614246	6.9572030	6.9514613	6.9446285
0.459375	6.9642115	6.9615889	6.9572758	6.9514029	6.9443835
0.415625	6.9644368	6.9617589	6.9573523	6.9513455	6.9441370
0.371875	6.9646699	6.9619349	6.9574326	6.9512894	6.9438893
0.328125	6.9649106	6.9621171	6.9575170	6.9512347	6.9436407
0.284375	6.9651592	6.9623057	6.9576055	6.9511815	6.9433920
0.240625	6.9654162	6.9625012	6.9576986	6.9511300	6.9431424
0.196875	6.9656818	6.9627038	6.9577963	6.9510804	6.9428993
0.153125	6.9659566	6.9629139	6.9578990	6.9510328	6.9426449
0.109375	6.9662410	6.9631318	6.9580069	6.9509448	6.9423975
0.065625	6.9665353	6.9633580	6.9581204	6.9509447	6.9421515
0.021875	6.9668401	6.9635929	6.9582397	6.9509044	6.9419073
.0000000	6.9669967	6.9637137	6.9583016	6.9508854	6.9417860

Table 7: Longitudinal Propagation Constant of Normal Modes at Different Inter-Waveguide Separation

Note: The waveguides are initially separated by 5.25 μm. In the merging process, there are totally 120 transition sections. The step size is 0.04375 μm throughout the transition region except on the two extreme ends with step size 0.021875 μm.

Bibliography

[1] A.A.M. Saleh and H.Kogelnik,"Reflective Sing-Mode Fiber-Optic Passive Star Couplers"*J.of Lightwave Tech.*,Vol.6,No.3,pp.392-398, Mar.1988.

[2] C. Dragone, "Efficient NxN Star couplers using Fourier optics." *J. of Lightwave Technol.*,vol. 7, Mar., 1989.

[3] K.Iwasaki, S.Karazono and K.Itakuna,"*The coupling of modes in three dielectric slab waveguides" Electron.,Commun.,Japan, vol58-c,no.8,pp.100-108, 1975.*

[4] D. Marcuse, *Theory of Dielectric Optical Waveguides*, New York:Academic, 1974.

[5] W.K.Burns, A.F. Miltons, A.B.Lee, E.J.West Applied optics 15, pp.1053-1063,1976.

[6] D.K.Cheng, *Field and Wave Electromagnetics*, 2nd Edition, Addison-wesley, New York, 1989.

[7] D. Lee, *Electromagnetic principles of Integrated Optics*, New York, John Wiley & Sons, 1986. Ch.2

[8] W.k. Burns,"Mode conversion in planar-dielectric separating waveguides," *IEEE J. of Quantum Electronics*, vol., QE-11, no.1, pp.32-39, Jan., 1975.

[9] R.G. Peall and R.A. Syms,"Comparison between strong coupling theory and experiment for three-arm directional couplers in Ti:LiNbO3" *IEEE J. of Lightwave Technol.*, vol.7, no.3, pp.540-554, Mar., 1989.

[10] K. Schinozaki, R. Fukunaga, and N. Watanabe,"Supermode control and phase front

measurements of phase-locked offset-coupled laser arrays with a large optical waveguide structure" *J. Appl. Phys.*, 66(3), pp.1057-1064, 1 Aug., 1989.

[11] J.P. Donnely, "*Three-guide optical couplers in GaAs*" *IEEE J. of Lightwave Technol.*, vol. LT-1, no.2, pp.417-423, Jun.,1983.

[12] M.A.Duguay, Y.Kokubun and T.L.Koch, "Antiresonant reflecting optical waveguides in Si02-si multilayer structures" *Appl.Phys.Lett.*,Vol 49,N0.7,pp.13-15,July 1986.

[13] M.Born and E.Wolf, "Principles of optics", Chapter 7, 3rd. Ed., New York: Pergamon,1965.

[14] N.S.Kapany and J.J.Burke, "Optical Waveguides"New York:Academic,1972.

[15] T.L.Koch,E.G.Burkhardt,F.G.Storz,T.J.Bridges and T.Sizer,"Vertically grating-coupling ARROW Structures for III-V integrated optics" *J.of Quantum Electron.*,Vol.QE-23,No.6,pp.889-897,June 1987.

[16] T.Baba, Y.Kokubun, T.Sakaki, and K.Iga,"Loss reduction of an ARRROW waveguide in shorter wavelength and its stack configuration", *J.of Lightwave Tech.*, Vol.6, No.9, pp.1440-1445,Sept. 1988.

[17] W.Y.Jiang and J. Chrostowski,"Analysis of ARROW",*Optics Lett.*

[18] W.V.McLevige,T.Itoh,and R.Mittra, "New Waveguide Structures for Millimeter-Wave and Optical Integrated Circuits,"*IEEE Trans. Microwave Theory Tech.*MTT-23,pp.788-794, Oct.,1975.

[19] C.Yeh, K.Ha,S.B.Dong, and W.P.Brown, Jr.. "Single-Mode optical Waveguides, "*Appl.Optics* 18, pp.1490-1504, May 1979.

[20] B.M.A.Rahman and J.B.Davies,"Finite-element analysis of optical and microwave waveguide problems,"*IEEE Trans.Microwave Theory Tech.*, MTT-32,pp-20-28,1984.

[21] K.S.Chang,"Finite element analysis of weakly guiding fibres with arbitrary refractive index distribution," *J.Lightwave Tech.*,vol.LT-4,pp.980-990, 1986.

[22] R.M.Knox and P.P.Toulios,"Integrated Circuits for the Millimeter through Optical Frequency Range,"*Proceedings,Symposium on Submillimeter Waves* (Polytechnic Press, Brooklyn,1970),pp.497-516, Mar.-April,1970.

[23] E.A.J.Marcatili,"Dielectric rectangular waveguide and directional coupler for integrated optics,"*Bell Syst.Tech.J*".,vol.48,pp.2071-2102,1969.

[24] G.B.Hocker and W.K.Burns,"Mode Dispersion in Diffused Channel Waveguides by Effective Index Method,"*Appl. Opt.*"16,pp.113-118,1977.

[25] S.T.Peng and A.A.Oliner,"Guidance and Leakage Properties of a Class of Open Dielectric Waveguides: Part I-Mathematical Formulations,"*IEEE Trans.Microwave Theory Tech.*MTT-29,pp.845-854,1981.

[26] A.A.Oliner, S.T.Peng,T.I.Hsu, and A.Sanchez,"Guidance and Leakage Properties of a Class of Open Dielectric Waveguides: Part II-New Physical Effects," *IEEE Trans.Microwave Theory Tech.*MTT-29,pp.855-869,1981.

[27] J.E. Goell,"A Circular-harmonic computer analysis of rectangular waveguide," *Beli*

Syst. Tech.J.,vol.48,pp.2133-2160,Sept.1969.

[28] K.S.Chiang,"Analysis of Optical Fibres by the Effective-Index Method,"*Appl. Opt.*25,pp.348-354,1986.

[29] K.S.Chiang,"Dual effective-index method for the analysis of rectangular dielectric waveguides,"*Appl.Opt*".,vol.25,pp.2169-2174,1986.

[30] K.S.Chiang,"Effective-index Method for the Analysis of Optical Waveguide Couplers and Arrays:An Asymptotic Theory,"*J.of Lightwave Tech.* ",Vol.9,No.1,pp.62-72,1991.

[31] K. Lee and W.steenaart,"NxN Passive Star Coupler based on the Exact Eigenmode Coupling and Diffraction Theory," *Proc. of the IEEE First International Workshop on Photonic Networks, Components & Applications*, Montebello. Canada, pp.321-325, October, 1990.

[32] J.C.Palais, *Fibre Optic Communications*, New Jersey, Prentice-Hall, second edition, 1989, chapter 4.

[33] J.K.Butler, D.E. Ackley, and D.Botez,"Coupled-mode analysis of phase-locked injection laser arrays" *Appl. Phys. Lett.* 44(3), pp.293-294, Feb,1984.

[34] E. Kapon, J. Katz and A. Yariv,"Supermode analysis of phase-locked arrays of semiconductor lasers" *Optics Letters*, pp.125-127, Apr.,1984.

[35] C. Dragone,"Efficiency of a periodic array with nearly ideal element pattern," *IEEE Photon., Technol., Lett.*, voll., no.8, pp.238-240, Aug., 1989.

[36] A.W. Synder and J.D. Love, *Optical Waveguide Theory*, London: Chapman and Hall, 1983, Ch.19.

[37] D. K. Cheng, *Field and Wave Electromagnetic*, Massuchusetts, Addision-Weslay, second edition, 1989. Ch.8.

[38] J.W. Goodman, *Introduction to Fourier Optics*, New York:McGraw-Hill, 1968. [39] C. Dragone, C. H. Henry, I. P. Kaminow, and R. C. Kistler, "Efficient multichannel integrated optics star coupler on silicon," IEEE Photo. Technol. Lett., vol.1, no.8, pp.241-243, Aug., 1989.